Molecular corridors and kinetic regimes in the multiphase chemical evolution of secondary organic aerosol

Manabu Shiraiwa[1,*], Thomas Berkemeier[1], Katherine A. Schilling-Fahnestock[2], John H. Seinfeld[2] & Ulrich Pöschl[1]

[1] Multiphase Chemistry Department, Max Planck Institute for Chemistry, 55128 Mainz, Germany.

[2] Division of Chemistry and Chemical Engineering, California Institute of Technology, Pasadena, CA91125, USA.

* Corresponding author (m.shiraiwa@mpic.de)

Last update: 16 June 2014

To be submitted to *ACP*

Abstract.

The dominant component of atmospheric organic aerosol is that derived from the oxidation of volatile organic compounds (VOCs), so-called secondary organic aerosol (SOA). SOA consists of a multitude of organic compounds, only a small fraction of which has historically been identified. Formation and evolution of SOA is a complex process involving coupled chemical reaction and mass transport in the gas and particle phases. Current SOA models do not embody the full spectrum of reaction and transport processes nor do they identify the dominant rate-limiting steps in SOA formation. Based on molecular identification of SOA oxidation products, we show here that the chemical evolution of SOA from a variety of VOC precursors adheres to characteristic "molecular corridors" with a tight inverse correlation between volatility and molar mass. The slope of these corridors corresponds to the increase in molar mass required to decrease volatility by one order of magnitude ($-\mathrm{d}M/\mathrm{dlog}C_0$). It varies in the range of 10-30 g mol^{-1} depending on the molecular size of the SOA precursor and the O:C ratio of the reaction products. Sequential and parallel reaction pathways of oxidation and dimerization or oligomerization progressing along these corridors pass through characteristic regimes of reaction-, diffusion-, or accommodation-limited multiphase chemical kinetics that can be classified according to reaction location, degree of saturation, and extent of heterogeneity of gas and particle phases. The molecular corridors and kinetic regimes help to constrain and described the properties of the products, pathways and rates of SOA evolution, thereby facilitating the further development of aerosol models for air quality and climate.

Introduction.

Organic aerosol is ubiquitous in the atmosphere and its major component is secondary organic aerosol (SOA) (Jimenez et al., 2009). Reaction of atmospheric VOCs with oxidants such as OH, O_3, and NO_3 initiate the formation of semi-volatile organic compounds (SVOCs), which can undergo further gas-phase oxidation to form low-volatility organic compounds (LVOCs) that will preferentially partition into the particle phase (Kroll and Seinfeld, 2008; Hallquist et al., 2009; Donahue et al., 2012). A fraction of the SVOCs partitions into the particle phase, wherein they can be transformed into LVOCs such as dimers, oligomers and other high molecular mass compounds (Jang et al., 2002; Kalberer et al., 2006; Ervens et al., 2011; Ziemann and Atkinson, 2012; Shiraiwa et al., 2013a). Some portion of the LVOCs can be transformed back to (semi-)volatile compounds or CO/CO_2 by fragmentation reactions triggered by OH or other oxidants at the particle surface or in the particle bulk (Bertram et al., 2001; Kroll and Seinfeld, 2008; Jimenez et al., 2009). SOA partitioning is also affected by particle-phase state, non-ideal thermodynamic mixing and morphology (Chang and Pankow, 2006; Zuend and Seinfeld, 2012; Shiraiwa et al., 2013b).

SOA consists of a myriad of organic compounds, of which only 10-30% have been identified (Goldstein and Galbally, 2007). Common techniques applied for the analysis of SOA are gas chromatography/electron impact ionization mass spectrometry (GC/EI-MS) and liquid chromatography/electrospray ionization mass spectrometry (LC/ESI-MS) (e.g., Surratt et al., 2006). Hard ionization, such as electron impact ionization, generally causes significant fragmentation of organic molecules, which makes molecular identification challenging, but can provide molecular structural information. The recent advent of soft ionization methods such as electrospray ionization (ESI), matrix-assisted laser desorption ionization (MALDI), atmospheric pressure chemical ionization (APCI), and direct analysis in real time (DART) ionization has facilitated the identification of the dominant fraction of the compounds constituting SOA by preserving analytes as intact or nearly intact during ionization (Kalberer et al., 2006; Williams et al., 2010; Laskin et al., 2012a; Laskin et al., 2012b; Chan et al., 2013; Nguyen et al., 2013; Vogel et al., 2013; Schilling-Fahnestock et al., 2014). This powerful methodology opens up a window onto the pathways of SOA formation and aging that was heretofore unavailable. Taking advantage of such data here we present a new 2D map for SOA evolution of molar

mass vs. volatility, which can be linked to kinetic regimes and reaction pathways of formation and aging of SOA that is currently poorly constrained and a major limitation in the understanding and prediction of atmospheric aerosol effects.

Molecular corridors for different SOA precursors.

Figure 1 shows 2D maps of molecular weight or molar mass (M) plotted against volatility or saturation mass concentration (C_0) for organic compounds in SOA from a range of anthropogenic and biogenic precursors: (a, b) dodecane (Yee et al., 2012), (c, d) cyclododecane, (e, f) hexylcyclohexane (Schilling-Fahnestock et al., 2014), (g) α-pinene (Docherty et al., 2005; Claeys et al., 2007; Claeys et al., 2009; Zuend and Seinfeld, 2012; Kahnt et al., 2014; Kristensen et al., 2014), (h) limonene (Jaoui et al., 2006; Kundu et al., 2012), (i) isoprene (Surratt et al., 2006; Surratt et al., 2010; Lin et al., 2012; Lin et al., 2013), (j) glyoxal and methylglyoxal (Lim et al., 2010; Sareen et al., 2010; Zhao et al., 2012). Experimental conditions including oxidants, NO levels and seed particles used in earlier studies are summarized in Table A1. The experimental conditions and methods applied in this study to analyze the formation and composition of SOA from C_{12} alkanes under low- and high-NO conditions are detailed in Appendix A and and Schilling-Fahnestock et al., (2014). DART is a soft ionization technique of atmospheric pressure ionization that has recently been used for the analysis of a variety of organic compounds with minimal fragmentation (Chan et al., 2013). SOA compounds identified include alcohols, ketones, aldehydes, hydroxycarbonyls, organic hydroperoxides and nitrates, which are generated in the gas phase (open markers), as well as dihydrofuran, furan, ether, ester, peroxyhemiacetal, hemiacetal, dimer, and imine, which are likely particle-phase products (Ziemann and Atkinson, 2012) (solid markers).

Vapor pressures and saturation mass concentrations of organic compounds were estimated using the EVAPORATION model ("Estimation of vapor pressure of organics, accounting for temperature, intramolecular, and non-additivity effects", (Compernolle et al., 2011). The EVAPORATION model estimates vapor pressure of molecules with the following functionalities: aldehyde, ketone, alcohol, ether, ester, nitrate, acid, peroxide, hydroperoxide, peroxy acyl nitrate and peracid. Organosulfates and imidazoles are not covered and were thus not included in our analysis, although they have been identified in SOA from biogenic precursors and glyoxal (Iinuma et al., 2007; Surratt et al., 2008; Ervens et al., 2011).

The markers in Fig. 1 are color-coded with atomic O:C ratio. Generally, volatility decreases and molar mass increases with chemical aging of SOA both in the gas and particle phases. Consequently, molar mass of oxidation products tightly correlates with volatility with high coefficient of determination (R^2) as summarized in Table 1. The 95% prediction intervals (dashed lines in Fig. 1) can be regarded as molecular corridors within which additional unidentified oxidation products are likely to fall. The negative slope of the fit lines corresponds to the increase in molar mass required to decrease volatility by one order of magnitude, $-dM/d\log C_0$. It increases from ~10 g mol^{-1} for glyoxal and methylglyoxal to ~25 g mol^{-1} for dodecane and cyclododecane, depending on the molecular size of the SOA precursor and the O:C ratio of the reaction products as will be discussed below. The mean value of $-dM/d\log C_0$ averaged over all investigated systems is 20±4 g mol^{-1}.

The composition of SOA may vary depending not only on the organic precursor but also on the oxidant and other reaction conditions of formation and aging (Presto et al., 2005; Surratt et al., 2006; Lin et al., 2012; Lin et al., 2013; Kristensen et al., 2014; Loza et al., 2014; Xu et al., 2014). The atomic O:C ratio tends to be higher at high NO concentrations, partly due to the formation of organonitrates (Nguyen et al., 2011; Schilling-Fahnestock et al., 2014). Even though Fig. 1(g), (h), (i) contain biogenic SOA oxidation products measured under different conditions as specified in Table A1, the molecular corridors are relatively tight with $R^2 > 0.85$. The molecular corridors of alkane SOA formed under low and high NO conditions are also quite similar (Figs 1a-f). Thus, the molecular corridors of SOA formation appear to be determined primarily by the organic precursor, and the extent to which they are influenced by reaction conditions warrants further studies.

Kinetic regimes and limiting cases.

Traditionally, SOA formation has been modeled based on instantaneous gas-particle equilibrium partitioning, implicitly assuming that gas-phase reactions are the rate-limiting step of SOA formation and growth (Pankow, 1994; Donahue et al., 2006; Hallquist et al., 2009). Recent studies, however, have shown that mass transport and chemical reaction in the particle phase may also play an important role (Fig. 2) (Ervens et al., 2011; Ziemann and Atkinson, 2012; Shiraiwa et al., 2013a). Recently, Berkemeier et al. (2013) provided a conceptual framework which enables the characterization of heterogeneous reactions and gas uptake in atmospheric aerosols

and clouds by a well-defined set of distinct kinetic regimes and limiting cases. We extended this framework to cover the complex interplay of gas- and particle-phase reactions in the evolution of SOA and enable a systematic classification of rate-limiting processes in the analysis and interpretation of laboratory chamber data and ambient measurements, as well as in the comparison of experimental results with theoretical predictions.

Different types of kinetic behavior can be characterized by three basic criteria as detailed in the Appendix B: (1) the location of the chemical reaction leading to SOA formation or aging (gas phase, particle surface, particle bulk), (2) the saturation ratio of the reactants (ratio of ambient concentration to saturation concentration), and (3) the extent of spatial heterogeneity of the gas and particle phases (concentration gradients). The kinetic regimes and limiting cases defined by these criteria can be visualized on a "kinetic cuboid", in which each axis corresponds to one of the three classification parameters as shown in Fig. 3(a). The symbols "G", "S", and "B" indicate the predominant reaction location: gas phase, particle surface, or particle bulk, respectively. A subscript denotes the rate-limiting process for SOA formation and aging: "rx" indicates chemical reaction; "bd" indicates bulk diffusion; "α" indicates mass accommodation; "gd" indicates gas-phase diffusion. Depending on atmospheric composition and reaction conditions, which vary widely in space and time, the chemical evolution of organic compounds and SOA particles can progress through any of these regimes.

The left part of the cuboid can be regarded as a particle-phase chemistry regime and the right side as a gas-phase chemistry regime. As shown in Fig. 3(b), the particle-phase chemistry regime (SB, including surface (S) or bulk (B) reaction) can be further subdivided into a reaction-diffusion regime (SB^{rd}), where the system is limited by reaction or diffusion in the particle-phase, and a mass-transfer regime (SB^{mt}) limited by mass accommodation at the interface or diffusion through the gas phase (Berkemeier et al., 2013). The gas-phase chemistry regime (G) comprises the traditional scenario of SOA formation determined by a rate-limiting chemical reaction in the gas phase followed by quasi-instantaneous gas-particle partitioning of the reaction products (G_{rx}), corresponding to so-called quasi-equilibrium growth (Shiraiwa and Seinfeld, 2012; Zhang et al., 2012). The rest of the gas-phase chemistry regime is mass transport-limited and corresponds to so-called non-equilibrium growth (Perraud et al., 2012; Zaveri et al., 2014), which can be kinetically limited by gas-to-

particle mass transfer (gas-phase diffusion and accommodation at the interface; G^{mt}) or retarded diffusion in the particle phase (G_{bd}).

Characteristic Pathways and Properties.

Figure 4(a) shows the ensemble of molecular corridors from Fig. 1 with a total of 909 identified oxidation products from seven different SOA precursors. They are constrained by two boundary lines corresponding to the volatility of *n*-alkanes C_nH_{2n+2} and sugar alcohols $C_nH_{2n+2}O_n$. These lines illustrate the regular dependence of volatility on the molar mass of organic compounds; the different slopes of 30 g mol^{-1} for C_nH_{2n+2} and 12 g mol^{-1} for $C_nH_{2n+2}O_n$ reflect that the decrease of volatility with increasing molar mass is stronger for polar compounds (see Fig. A4 for alternative representation).

Many early generation gas-phase oxidation products of alkanes as well as dimers or oligomers with low O:C ratio (LOC) fall into a molecular corridor close to the C_nH_{2n+2} line, which we designate as LOC corridor ($-dM/d\log C_0 \geq$ ~25 g mol^{-1}, blue shaded area). Aqueous-phase reaction and autoxidation products with high O:C ratio (HOC), on the other hand, tend to fall into a corridor near the $C_nH_{2n+2}O_n$ line, which we designate as HOC corridor ($-dM/d\log C_0$ of $\leq$ ~15 g mol^{-1}, red shaded area). The area in between is characterized by intermediate O:C ratios and accordingly designated as IOC corridor ($-dM/d\log C_0 \approx$ ~20 g mol^{-1}). Among the SOA systems investigated in this study, the small precursor VOCs glyoxal, methylglyoxal and isoprene (C_2-C_5) evolve through the HOC corridor, and the terpenes α-pinene and limonene (C_{10}) through the IOC corridor. The alkanes dodecane and cyclododecane (C_{12}) evolve through the LOC corridor, while hexylcyclohexane exhibits a branching between the LOC and HOC corridors, suggesting the involvement of different reaction pathways. For unidentified SOA products, the molecular corridor ensemble in Fig. 4(a) and alternative representations (Fig. A4(a)) may also be used as a look-up plot to obtain a rough estimate of volatility by comparison of molar mass and O:C ratio (e.g., from soft-ionization high-resolution mass spectrometry) to the data in the plot.

Characteristic reaction pathways and relevant kinetic regimes are outlined in Fig. 4(b). SOA precursor VOCs with high volatility and low molar mass are located in the lower right corner of the molecular corridor ensemble. As illustrated in the insert in Fig. 4(b), single-step functionalization usually leads to a small increase in

molar mass, corresponding to one order of decrease in volatility (Donahue et al., 2006), while dimerization and oligomerization tend to multiply molar mass, and thus decrease volatility by multiple orders of magnitude (Trump and Donahue, 2014) (e.g., three to four orders of magnitude for alkane and terpene SOA, see Fig. 1). Fragmentation, on the other hand, can lead to a substantial decrease of molar mass and increase in volatility (Bertram et al., 2001; Yee et al., 2012; Schilling-Fahnestock et al., 2014). As a result, simple gas-phase oxidation products are confined to the lower right area in the 2D space. Such oxidation products ($C_0 > 10$ μg m^{-3}) tend to fall into the gas-phase reaction limiting case G_{rx} (quasi-equilibrium growth), as their gas-particle equilibration timescale is on the order of seconds to minutes (Shiraiwa and Seinfeld, 2012) (see Appendix C&D).

Particle-phase dimerization and oligomerization involving two or more molecules usually leads to the formation of compounds with low volatility and high molar mass lying in the upper left area in the 2D space. The formation of such particle-phase products is likely limited by reaction or diffusion in the particle bulk (SB^{rd}), as rate coefficients for dimer formation are relatively low (< 10 M^{-1} s^{-1}) (Ziemann and Atkinson, 2012) and large molecules tend to diffuse slowly (Pfrang et al., 2011; Shiraiwa et al., 2011; Abramson et al., 2013; Zhou et al., 2013). An example of reaction pathways leading to dimerization is shown in Fig. 5 for dodecane SOA (Appendix D, Shiraiwa et al., 2013a). Within the molecular corridor of dodecane SOA evolution, Fig. 5 illustrates a specific trajectory from the precursor (dodecane, 0) through multiple generations of surrogate products of gas-phase oxidation and functionalization (multifunctional alcohols, ketones, and peroxides, 1-5), gas-phase fragmentation (aldehydes, 6), and particle-phase dimerization between aldehydes and peroxides to peroxyhemiacetals (7). Numerical model results shown in Fig. A2 indicate that the trajectory of chemical evolution passes through different kinetic regimes, i.e., from limitation by gas-phase reaction (G_{rx}) to particle-phase reaction and diffusion (SB^{rd}). Note that particle-phase reactions may also be limited by gas-to-particle mass transfer (e.g., accommodation, supply of reactive gases into the particle), when they are sufficiently fast, such as catalyzed by acids (Jang et al., 2002; Iinuma et al., 2004; Offenberg et al., 2009; Surratt et al., 2010).

Aqueous-phase processing of glyoxal and methylglyoxal is an efficient pathway for formation of low volatility and semi-volatile HOC compounds (Liggio et al., 2005; Carlton et al., 2007; Lim et al., 2010; Ervens et al., 2011; Zhao et al., 2012).

Uptake of glyoxal into the particle phase leads to hydration and acid catalysis to form hemiacetals, aldols, imines, anhydrides, esters and organosulfates (Lim et al., 2010). Reactive uptake of isoprene epoxydiols (IEPOX) and subsequent formation of oligomers (Surratt et al., 2010; Lin et al., 2012; Lin et al., 2013) also progresses over the HOC corridor. Whether multiphase chemistry of glyoxal and IEPOX is limited by mass transfer or chemical reactions may depend on various factors including reaction rate coefficients, relative humidity, particle pH, and Henry's law constant (Ervens and Volkamer, 2010; McNeill et al., 2012; Kampf et al., 2013).

Recently, highly oxidized extremely low volatility organic compounds (ELVOC) have been detected in field and chamber experiments (Ehn et al., 2012; Schobesberger et al., 2013; Ehn et al., 2014). Such compounds may populate the upper left corner of the HOC corridor. It has been shown that such compounds can be formed via autoxidation (inter- and intramolecular hydrogen abstraction by peroxy radicals) in the gas and particle phases (Crounse et al., 2013). When they are formed in the gas phase, the equilibration timescale of partitioning is long due to their low volatility and the SOA growth is limited most likely by mass transfer (gas-phase diffusion and accommodation; G^{mt}) (see Appendix C and Fig. A2) (Pierce et al., 2011; Riipinen et al., 2011; Shiraiwa and Seinfeld, 2012). Note that kinetic limitation by retarded bulk diffusion (G_{bd}) is also possible for semi-volatile and low volatility products, when organic particles adopt amorphous solid state (Virtanen et al., 2010; Cappa and Wilson, 2011; Shiraiwa et al., 2011; Vaden et al., 2011; Kuwata and Martin, 2012; Perraud et al., 2012; Shiraiwa and Seinfeld, 2012; Renbaum-Wolff et al., 2013; Zaveri et al., 2014). Indeed, recent observation found that some SVOCs do not necessarily adhere to equilibrium partitioning (Vogel et al., 2013).

Formation of high molecular weight SOA compounds from oligomerization or autoxidation results in high average molar mass for the biogenic systems of isoprene and α-pinene (Kalberer et al., 2006) as well as the anthropogenic C_{12} alkanes (Fig. 1 and Tab. 1; Schilling-Fahnestock et al., 2014). Figure 4(a) shows that most identified oxidation products with molar masses higher than 300 g mol^{-1} are particle-phase products (solid markers). Thus, the relatively high average molar mass observed for laboratory-generated SOA points to the importance of particle-phase chemistry in these systems. Some SOA compounds with higher molar mass are gas-phase oxidation products including ELVOC and ester dimers observed in α-pinene

oxidation (Ehn et al., 2014; Kristensen et al., 2014), and there are also some particle-phase products with relatively low molar mass including furans and dihydrofurans in dodecane and cyclododecane SOA (Yee et al., 2012; Loza et al., 2014) as well as glyoxal and IEPOX products in isoprene SOA (Lim et al., 2010; Surratt et al., 2010). Nevertheless, the clustering of identified reaction products in molecular corridors may facilitate estimation of the relative importance of gas- vs. particle-phase routes to SOA formation (Fig. 1).

Molar mass and O:C ratio also correlate with the glass transition temperature of organic compounds, which tends to increase with increasing molar mass and O:C ratio (Koop et al., 2011). As elevated glass transition temperatures are indicative of semi-solid or amorphous solid states, SOA evolution represented in molecular corridors allows one to infer the regime, in which particles are likely to become highly viscous. For example, recent experiments have shown an order of magnitude increase in the viscosity of oleic acid particles upon reaction with ozone owing to formation of oligomers (Hosny et al., 2013), and model calculations indicate that this may lead to the formation of surface crusts (Pfrang et al., 2011).

In summary, presenting identified SOA products in a molecular corridor encapsulates fundamental aspects of SOA formation and aging: volatility, molar mass, O:C ratio, and phase state. Such a representation can be used to constrain/predict the properties of unidentified SOA oxidation products. The kinetic regimes, within which SOA evolution is occurring along the molecular corridor, facilitate the specification of the rate of progression to higher generation products. Thus, molecular corridors may serve as a basis for compact representation of SOA formation and aging in regional and global models of climate and air quality.

306 **Appendix A. Product analysis of alkane SOA**

307 Photo-oxidation and subsequent SOA formation of *n*-dodecane,
308 cyclododecane, and hexylcyclohexane was conducted in the 28 m^3 Teflon reactors in
309 the Caltech Environmental chamber (Yee et al., 2012; Loza et al., 2014; Schilling-
310 Fahnestock et al., 2014). Aqueous H_2O_2 solution was evaporated into the chamber as
311 the OH source, followed by the atomization of an aqueous ammonium sulfate solution
312 generating seed particles, which were subsequently dried. Experiments were
313 conducted under low-NO conditions, in which alkyl peroxy radicals (RO_2) react
314 primarily with HO_2, and under high-NO conditions, in which RO_2 react primarily
315 with NO (Loza et al., 2014).

316 SOA particles were collected on Teflon filters (Pall Life Sciences, 47 mm, 1.0
317 μm pore size). Off-line analysis of collected particles was conducted by solvent
318 extraction and gas chromatography time-of-flight mass spectrometry (GC-TOF-MS,
319 GCT Premier, Waters) and GC/ion trap mass spectrometry (Varian Saturn 2000,
320 Agilent), and by direct analysis in real time (DART)- time-of-flight and ion trap mass
321 spectrometry (DART-AccuToF, JEOL USA; Caltech Mini-DART; LTQ, Thermo
322 Fisher). Further details on experimental conditions and analytical methods can be
323 found in Schilling-Fahnestock et al. (2014).

324 The average molar mass of SOA was estimated by taking the sum of the
325 product of the percent relative concentration of each compound with respect to the
326 internal standard (dibutyl phthalate present in each filter) by each compound's molar
327 mass. The relative concentration for each compound was obtained through the
328 relationship of ion current intensity and concentration for DART-MS. In DART
329 analysis, ion current intensity (I) is proportional to the concentration (C), vapor
330 pressure (P_{vap}) and proton affinity (A): $I = AP_{vap}C$. This equation is written for both
331 the analyte and the internal standard and then the ratio was calculated, which allows
332 for the cancellation of the proton affinity term. Analyte vapor pressures were
333 estimated by using proposed structures based on HR-MS data-derived formulae and
334 known mechanisms with the EVAPORATION (Estimation of vapor pressure of
335 organics, accounting for temperature, intramolecular, and non-additivity effects)
336 model (Compernolle et al., 2011). When rewritten to solve for the relative
337 concentration of the analyte with respect to the concentration of the internal standard,
338 the equation becomes:

$$\frac{C_A}{C_{IS}} = \frac{P_{vap,IS}}{P_{vap,A}} \frac{I_A}{I_{IS}}$$

Atomic O:C ratio vs. volatility is used to represent formation and aging of SOA (Jimenez et al., 2009; Donahue et al., 2011). By analogy to Figs. 1 and 4, major oxidation products are shown in Figures S1 and S2. The markers are color coded by molar mass. Upon gas-phase oxidation, volatility decreases and O:C ratio increases, leading to a linear correlation in O:C ratio vs. volatility for gas-phase oxidation products. Particle-phase products, however, exhibit generally lower volatility and O:C ratio as compared to gas-phase oxidation products. Consequently, the overall correlation between O:C ratio and volatility for the full spectrum of SOA products has a low coefficient of determination and wide prediction interval (Table 1, Figure S1). Figure S2 shows the summary of O:C ratio vs. volatility, showing that the oxidation products cover almost the full area in this 2D space. Clear trend is found that volatile compounds have low molar mass, whereas low volatility compounds with low O:C ratio have high molar mass.

Appendix B. Kinetic regimes for SOA formation

Figure A1 shows a classification scheme for kinetic regimes and limiting cases for SOA formation and aging. Note that the term *limiting case* is reserved for a system that is governed by a single, clearly defined limiting process; the term *kinetic regime* designates a system that is governed by a few (often only one or two) clearly defined rate-limiting processes (Berkemeier et al., 2013). The classification within the particle phase regime (right-hand side of Fig. 3) is explained in detail by Berkemeier et al. (2013). In this study, the gas-phase regime (left-hand side of Fig. 3) extends the classification scheme to SOA formation. The cases of limiting behavior arise from three criteria that are fundamental to formation and partitioning of an oxidation product: 1) the location (gas phase, particle surface, particle bulk) of the reaction leading to SOA formation, 2) the species' saturation ratio (ratio of ambient concentration to saturation concentration) of the oxidation products, and 3) the extent of spatial heterogeneity of the gas and particle phases. Identifying kinetic regimes and limiting cases can be facilitated by an aerosol model, such as the kinetic multi-layer model for gas-particle interactions (KM-GAP) that explicitly resolves mass transport and chemical reactions in the gas and particle phases (Shiraiwa et al., 2012).

372 **B.1. Criterion 1: Reaction location (Gas vs. Surface vs. Bulk)**

373 *Where does formation of oxidation products that contribute to SOA mass*
374 *predominantly occur, gas phase, particle surface or particle bulk?* A two-pronged
375 criterion can be developed. The first sub-criterion evaluates the relative contribution
376 of gas- vs. particle-phase chemistry. The gas- vs. particle-phase contribution ratio
377 (GPCR) can be defined as ratio of the production rate of the oxidation product in the
378 gas phase (P^g) to the total production rate in gas and particle phases (P^g+P^p):

379 $$\mathrm{GPCR} = P^g / (P^g + P^p) \quad (1)$$

380 As GPCR approaches unity, an oxidation product is produced primarily in the gas
381 phase; and as GPCR approaches zero, it is primarily produced in the particle phase.

382 If particle-phase chemistry dominates (GPCR ≈ 0), the surface to total particle
383 phase contribution ratio (STCR) is used to assess the extent to which production
384 occurs predominantly at the surface or in the bulk. STCR can be calculated using the
385 production rate of the oxidation product at the surface (P^s) and in the particle bulk
386 (P^b):

387 $$\mathrm{STCR} = P^s /(P^s + P^b) \quad (2)$$

388 If the particle-phase reaction primarily occurs at the surface, STCR approaches unity;
389 and STCR approaches zero if the reaction occurs primarily in the bulk.

390

391 **B.2. Criterion 2: Saturation ratio**

392 *Is mass transfer of an oxidation product through the gas or into the particle*
393 *phase limiting SOA growth?* After determination of the reaction location, this
394 criterion further classifies the system based on the abundance of oxidation products at
395 the particle surface versus in the near-surface bulk.

396 In the gas-phase regime, the surface saturation ratio (SSR) can be used to
397 judge the extent to which kinetic limitation of mass transport occurs in the gas phase.
398 With this parameter, the surface concentration of an oxidation product Z, $[Z]_s$, is
399 compared to its surface saturation concentration $[Z]_{s,sat}$. In the absence of reaction or
400 diffusion into the bulk, $[Z]_{s,sat}$ is determined by the gas-phase concentration of Z, $[Z]_g$,
401 and the rates of adsorption and desorption k_a and k_d: $[Z]_{s,sat} = k_a / k_d [Z]_g$ (Pöschl et al.,
402 2007; Berkemeier et al., 2013). The SSR is defined as the ratio of $[Z]_s$ to its saturation
403 concentration at adsorption equilibrium:

404 $$\mathrm{SSR} = [Z]_s /[Z]_{s,sat} \quad (3)$$

The numerical interpretation of SSR is: 1) As SSR approaches zero, the surface is starved of Z, and the system is limited by mass transfer (G^{mt} regime) either by gas-phase diffusion (G_{gd} limiting case) or surface accommodation (G_{α} limiting case). As SSR approaches unity, the surface is adequately supplied with Z and the system can be limited by production of Z in the gas phase (G_{rx} limiting case) or mass transport into the bulk (G_{bd} limiting case).

In the particle-phase regime, the classification step is based on SSR or the bulk saturation ratio (BSR) to distinguish between systems in the reaction-diffusion regime or the mass-transfer regime (Berkemeier et al., 2013). The BSR is defined analogously to SSR as the ratio of near-surface bulk concentration of an oxidation product to its saturation concentration.

B.3. Criterion 3: Mixing Parameters (MP)

Is SOA growth limited by diffusion in the gas or particle phase? Depending on the reaction location and saturation ratio, mixing parameters are used to assess the heterogeneity of the gas-particle system. One can define the surface mixing parameter (SMP), the bulk mixing parameter (BMP), the gas-phase diffusion correction factor (C_g), and the gas-particle mixing parameter (GMP). SMP is defined as the ratio of the actual surface concentration of compound i to the maximum possible surface concentration in the case of perfect particle-phase mixing. BMP is defined using an effective reacto-diffusive length (Berkemeier et al., 2013). As a MP approaches zero, a strong concentration gradient exists and the system is limited by diffusion; as MP approaches unity, the system is well-mixed and limited by reaction.

In mass-transfer limited systems (indicated by a low SR), $C_{g,i}$ distinguishes between gas-phase diffusion limitation and accommodation limitation. $C_{g,i}$ is defined as the ratio of the concentration of compound i in the near-surface gas phase (one mean free path away from the surface) to that in the gas phase far from the particle (Pöschl et al., 2007):

$$C_{g,i} = C_i^{gs} / C_i^{g} \quad (4)$$

As $C_{g,i}$ approaches zero, the compound i exhibits a strong concentration gradient in the gas phase and the system is classified as gas-phase diffusion limited (G_{gd} limiting case); as $C_{g,i}$ approaches unity, the system is designated as accommodation-limited (G_{α} limiting case).

The gas-particle mixing parameter (GPMP) measures the extent to which the gas-particle system is in quasi-equilibrium and is defined as the ratio of equilibrium gas-phase mass concentration of compound i, $C_i^{g,eq}$, to gas-phase mass concentration, C_i^{g} (far from particle), which is equivalent to the ratio of particle-phase mass concentration, C_i^{PM}, to equilibrium particle-phase mass concentration, $C_i^{PM,eq}$:

$$GPMP_i = C_i^{g,eq} / C_i^{g} = C_i^{PM} / C_i^{PM,eq} \quad (5)$$

$C_i^{g,eq}$ and $C_i^{PM,eq}$ can be calculated using an equilibrium partitioning theory (Pankow, 1994; Donahue et al., 2006):

$$C_i^{g,eq} = C_i^{*} C_i^{PM} / C_{Tot} \quad (6)$$

$$C_i^{PM,eq} = C_i^{g} C_{Tot} / C_i^{*} \quad (7)$$

where C_i^{*} is the effective saturation mass concentration of compound i and C_{Tot} is the total particle mass concentration. In the case of ideal mixing, C_i^{*} is equal to the gas-phase saturation mass concentration over the pure subcooled liquid (C_i^{0}). Note that $C_i^{g,eq}$ can be regarded as a gas-phase mass concentration just above the particle surface, C_i^{s}, when Raoult's law is strictly obeyed and C_i^{s} is in equilibrium with the whole particle (i.e., usually the case for liquid particles).

The value of GPMP determines the extent to which SOA growth is controlled by quasi-equilibrium growth or mass transport limited growth. $C_i^{g} = C_i^{g,eq}$ (or $C_i^{PM} = C_i^{PM,eq}$) at gas-particle equilibrium. The particle still grows, if C_i^{g} changes slowly and $C_i^{g,eq}$ follows C_i^{g} instantaneously (quasi-equilibrium growth) (Shiraiwa and Seinfeld, 2012; Zhang et al., 2012). If $C_i^{g} > C_i^{g,eq}$, compound i will diffuse from the gas to the particulate phase, driven by concentration or partial pressure gradient between the gas and particle phases (non-equilibrium or mass transport limited growth). Thus, the numerical interpretation of GMP is: 1) As GPMP approaches 0, SOA growth is limited kinetically by mass transport; 2) As GPMP approaches unity, SOA growth is in quasi-equilibrium and the system is subject to the gas-phase reaction limitation case G_{rx} (the system is limited only by the gas-phase formation rate).

Note that GPMP is small for the limiting cases of G_{bd}, G_{α}, and G_{gd}. In these limiting cases, SOA growth is still sensitive to the gas-phase formation rate (as it determines the gas-phase concentration), but is limited by interfacial transport, which comprises gas-phase diffusion, surface accommodation, and surface-to-bulk transport processes. Gas-phase diffusion and surface accommodation limitation can be differentiated from surface-to-bulk transport limitation either by SSR or by comparing surface (α_s) and bulk (α_b) accommodation coefficients, each of which is resolved by

KM-GAP. α_s is defined as the probability of a molecule sticking to the surface upon collision, whereas α_b is defined as the respective probability of a molecule to enter the bulk of the particle (Pöschl et al., 2007; Shiraiwa et al., 2012). If $\alpha_s \approx \alpha_b$, then interfacial transport is not limited by surface-to-bulk exchange and thus is limited by either gas-phase diffusion or surface accommodation; if $\alpha_s > \alpha_b$, then the interfacial transport is limited by surface-to-bulk transport, (dissolution or bulk diffusion). For additional discussion of accommodation vs. surface-bulk exchange see Appendix C in Berkemeier et al. (2013).

Appendix C. Examples of kinetic regimes and limiting cases

Here we use KM-GAP to model condensation of a semi-volatile compound generated by oxidation of a parent VOC. We assume that the parent VOC with an initial concentration of 10^{10} cm^{-3} is converted to a semi-volatile product with a first-order rate coefficient of 0.1 min^{-1}. Conversion of the first-generation product to higher generation products and particle-phase reactions need not be considered. The initial number and mass concentrations of non-volatile pre-existing particles are taken as 10^3 cm^{-3} and 0.1 µg m^{-3}, respectively. The initial particle size distribution is assumed log-normal with mean diameter of 50 nm and a standard deviation of 1.5. The required kinetic parameters for the simulation are given in Table A2. Gas-phase diffusion coefficient (D_g) of an oxidation product is varied between 0.01 – 0.05 cm^2 s^{-1} (Bilde et al., 2003; Bird et al., 2007). Surface accommodation coefficient ($\alpha_{s,0}$) and bulk diffusion coefficient (D_b) are also varied to illustrate the different kinetic regimes and limiting cases for SOA formation in the gas-phase regime.

Figure A2 shows the results of such simulation. The temporal evolution of mass concentration of the parent VOC (black), the oxidation product in the gas phase (C^g, solid blue), in the near-surface gas phase (C^{gs}, dotted blue), in the particle phase (C^{PM}, red), and equilibrium gas-phase concentration ($C^{g,eq}$, dashed blue) are shown. In the simulation presented in Figure A2a, SOA growth is limited by mass transfer, namely gas-phase diffusion and accommodation (G^{mt} regime, lying between limiting cases G_{gd} and G_α) up to ~10 s, indicated by a low surface saturation ratio (SSR) and a low the gas-phase diffusion correction factor ($C_g = C^g / C^{gs} \approx 0.7$). The gas-phase concentration gradient vanishes within ~10 s ($C^g \approx C^{gs}$), and as C^g continues to increase due to the conversion of the parent VOC, $C^{g,eq}$ follows the change in C^g

essentially instantaneously and C^{P} increases. In this case, the gas-phase rate of formation of the oxidation product controls particle growth corresponding to the limiting case of G_{rx} (so-called quasi-equilibrium growth) (Shiraiwa and Seinfeld, 2012; Zhang et al., 2012).

In the simulation presented in Figure A2b with a relatively low surface accommodation coefficient of 10^{-3}, a steep concentration gradient exhibits between the gas phase and the particle surface ($C^{g} \approx C^{gs} > C^{g,eq}$) during SOA growth. The system is limited by accommodation (G_{α}), as SSR is low but C_g is 1. Figure A2c shows the corresponding results for particles in an amorphous semi-solid state with the low bulk diffusion coefficient of 10^{-17} cm^2 s^{-1}. In this case, particle growth is limited by surface-to-bulk transport (G_{bd}), as SSR is high and GPMP is low. Note that GPMP refers to the gap between C^{g} and $C^{g,eq}$. The bulk accommodation coefficient α_b is ~10^{-5}, much smaller than the surface accommodation coefficient α_s. Sensitivity studies with varying D_b reveal that when D_b < ~10^{-15} cm^2 s^{-1} the timescales for surface-bulk exchange and bulk diffusion become longer than that of gas-phase diffusion and accommodation (Shiraiwa and Seinfeld, 2012). From the Stokes-Einstein relation, this value corresponds to a viscosity of ~10^{7} Pa s, which is on the same order as the viscosity of α-pinene SOA at 40 % RH (Renbaum-Wolff et al., 2013). Thus, SOA growth can be limited by bulk diffusion at low RH; whereas surface accommodation becomes more important at high RH.

Figure A2d shows the simulation for gas-phase formation and partitioning of low volatility oxidation products (C_0 = 10^{-3} μg m^{-3}) into liquid particles. SSR is low over the course of particle growth, indicating persistence of a strong concentration gradient between the gas phase and the particle surface. The gas-phase diffusion correction factor (C_g) stays at 0.7 up to ~10^{3} s, indicating that near-surface gas phase concentration $[Z]_{gs}$ is depleted by 30% compared to gas phase concentration $[Z]_{g}$ due to rapid uptake and slow gas diffusion (D_g = 0.01 cm^2 s^{-1}). C_g decreases substantially down to ~0.2 only when gas-phase formation ceases at ~10^{3} - 10^{4} s. Overall, SOA growth is limited by mass transfer (gas-phase diffusion and accommodation; G^{mt} regime). When a very low bulk diffusivity is assumed ($D_b \approx 10^{-19}$ cm^2 s^{-1}; figure not shown), SSR is close to 1 and GPMP is very low during particle growth; thus the system is limited by bulk diffusion (G_{bd}). Consequently, partitioning of low volatility

compounds could be limited by bulk diffusion, when organic particles adopt amorphous solid state (Shiraiwa and Seinfeld, 2012; Zaveri et al., 2014).

Appendix D. Application to chamber data: Dodecane photooxidation

Here we apply the classification scheme to experimental data on SOA formation from oxidation of the C_{12} alkane, dodecane ($C_{12}H_{28}$) in the Caltech Environmental Chamber (Yee et al., 2012). 34 ppb dodecane was oxidized by OH radicals over 20 hours in the presence of dry ammonium sulfate seed particles at low concentrations of NO_x typical of nonurban conditions. KM-GAP was used to simulate the evolution of SOA mass, the organic atomic oxygen-to-carbon (O:C) ratio, and particle-size distribution in the chamber experiments (Shiraiwa et al., 2013a). In the gas phase, SVOCs resulting from up to five generations of OH oxidation are considered. Some of the fourth generation products have been established to be multifunctional carbonyl compounds (aldehydes) that can react in the particle phase with hydroperoxide, hydroxyl, and peroxycarboxylic acid groups, forming peroxyhemiacetal (PHA), hemiacetal, and acylperoxyhemiacetal, respectively (Docherty et al., 2005; Yee et al., 2012; Ziemann and Atkinson, 2012). The observed evolution of the particle size distribution is simulated successfully, only if such particle-phase chemistry is included (Shiraiwa et al., 2013a).

Figure 5 shows the span of molar mass and gas-phase saturation concentrations over the pure subcooled liquids (C_i^0) for gas-phase oxidation products and particle-phase products of the dodecane system. The smaller symbols indicate individual products predicted in the dodecane photooxidation chemical mechanism (Yee et al., 2012) and the large solid circles indicate the surrogate compounds used in the KM-GAP simulations (Shiraiwa et al., 2013a). Upon gas-phase multi-generation oxidation, the volatility of SVOCs decreases from ~10^6 μg m^{-3} (dodecane) to ~1 μg m^{-3}. The particle-phase products have significantly lower volatilities of ~10^{-2} μg m^{-3}.

Figures. A3a and b show the temporal evolution of mass concentration of the 1st and 5th generation oxidation products in the gas phase (C^g), at the particle surface (C^s), and in the particle phase (C^{PM}). C^g is slightly higher than $C^{g,eq}$ up to ~5 h due to continuous generation of oxidation products in the gas phase, and eventually reaching $C^g \approx C^{g,eq}$ for both products (GMP ≈ 1). Note that mass concentration in the near surface gas phase (C^{gs}) is identical to C^g, indicating that gas-phase diffusion is not a

limiting step. The same trend is seen for other generation products. Thus, the contribution of gas-phase semi-volatile oxidation products to SOA formation is limited by their formation in the gas phase, corresponding to the limiting case of G_{rx}.

Particle-phase products are formed by the reaction of reactive aldehydes with SVOCs in the particle phase. Simulations suggest that this reaction occurs mainly at the surface and in the near-surface bulk (Shiraiwa et al., 2013a). Aldehydes and SVOCs are both saturated in the bulk (BSR is high). A strong concentration gradient of aldehydes in the bulk is predicted, whereas SVOCs are predicted to be essentially homogeneous in the bulk ($BMP_{XY} \approx 0.5$). Bulk reaction is tightly coupled with bulk diffusion and the system falls into the reaction-diffusion regime (SB^{rd}), particularly the traditional reacto-diffusive case (B^{rd}_{trad}) (Worsnop et al., 2002; Pöschl et al., 2007; Kolb et al., 2010; Berkemeier et al., 2013).

Acknowledgements.

This work was funded by the Max Planck Society and U.S. National Science Foundation grant AGS-1057183. MS, TB, and UP thank the European Commission project Pan-European gas-aerosols-climate interaction study (No. 265148, PEGASOS). MS thanks the Japan Society for the Promotion of Science (JSPS) for Postdoctoral Fellowships for Research Abroad.

References.

Abramson, E., Imre, D., Beranek, J., Wilson, J. M., and Zelenyuk, A.: Experimental determination of chemical diffusion within secondary organic aerosol particles, Phys. Chem. Chem. Phys., 15, 2983-2991, 2013.

Berkemeier, T., Huisman, A. J., Ammann, M., Shiraiwa, M., Koop, T., and Pöschl, U.: Kinetic regimes and limiting cases of gas uptake and heterogeneous reactions in atmospheric aerosols and clouds: a general classification scheme, Atmos. Chem. Phys., 13, 6663-6686, 2013.

Bertram, A. K., Ivanov, A. V., Hunter, M., Molina, L. T., and Molina, M. J.: The reaction probability of OH on organic surfaces of tropospheric interest, J. Phys. Chem. A, 105, 9415-9421, 2001.

Bilde, M., Svenningsson, B., Monster, J., and Rosenorn, T.: Even-odd alternation of evaporation rates and vapor pressures of C3-C9 dicarboxylic acid aerosols, Environ. Sci. Technol., 37, 1371-1378, 2003.

Bird, R. B., Stewart, W. E., and Lightfoot, E. N.: Transport Phenomena (2nd Ed.), John Wiley & Sons, Inc., New York, 2007.

606 Cappa, C. D., and Wilson, K. R.: Evolution of organic aerosol mass spectra upon heating:
607 implications for OA phase and partitioning behavior, Atmos. Chem. Phys., 11, 1895-
608 1911, 2011.

609 Carlton, A. G., Turpin, B. J., Altieri, K. E., Seitzinger, S., Reff, A., Lim, H. J., and Ervens, B.:
610 Atmospheric oxalic acid and SOA production from glyoxal: Results of aqueous
611 photooxidation experiments, Atmos. Environ., 41, 7588-7602, 2007.

612 Chan, M. N., Nah, T., and Wilson, K. R.: Real time in situ chemical characterization of sub-
613 micron organic aerosols using Direct Analysis in Real Time mass spectrometry (DART-
614 MS): the effect of aerosol size and volatility, Analyst, 138, 3749-3757, 2013.

615 Chang, E. I., and Pankow, J. F.: Prediction of activity coefficients in liquid aerosol particles
616 containing organic compounds, dissolved inorganic salts, and water - Part 2:
617 Consideration of phase separation effects by an X-UNIFAC model, Atmos. Environ., 40,
618 6422-6436, 2006.

619 Claeys, M., Szmigielski, R., Kourtchev, I., Van der Veken, P., Vermeylen, R., Maenhaut, W.,
620 Jaoui, M., Kleindienst, T. E., Lewandowski, M., Offenberg, J. H., and Edney, E. O.:
621 Hydroxydicarboxylic acids: Markers for secondary organic aerosol from the
622 photooxidation of alpha-pinene, Environ. Sci. Technol., 41, 1628-1634, 2007.

623 Claeys, M., Iinuma, Y., Szmigielski, R., Surratt, J. D., Blockhuys, F., Van Alsenoy, C., Boege,
624 O., Sierau, B., Gomez-Gonzalez, Y., Vermeylen, R., Van der Veken, P., Shahgholi, M., Chan,
625 A. W. H., Herrmann, H., Seinfeld, J. H., and Maenhaut, W.: Terpenylic Acid and Related
626 Compounds from the Oxidation of alpha-Pinene: Implications for New Particle
627 Formation and Growth above Forests, Environ. Sci. Technol., 43, 6976-6982, 2009.

628 Compernolle, S., Ceulemans, K., and Muller, J. F.: EVAPORATION: a new vapour pressure
629 estimation methodfor organic molecules including non-additivity and intramolecular
630 interactions, Atmos. Chem. Phys., 11, 9431-9450, 2011.

631 Crounse, J. D., Nielsen, L. B., Jørgensen, S., Kjaergaard, H. G., and Wennberg, P. O.:
632 Autoxidation of organic compounds in the atmosphere, J. Phys. Chem. Lett., 4, 3513-
633 3520, 2013.

634 Docherty, K. S., Wu, W., Lim, Y. B., and Ziemann, P. J.: Contributions of organic peroxides
635 to secondary aerosol formed from reactions of monoterpenes with O_3, Environ. Sci.
636 Technol., 39, 4049-4059, 2005.

637 Donahue, N. M., Robinson, A. L., Stanier, C. O., and Pandis, S. N.: Coupled partitioning,
638 dilution, and chemical aging of semivolatile organics, Environ. Sci. Technol., 40, 2635-
639 2643, 2006.

640 Donahue, N. M., Epstein, S. A., Pandis, S. N., and Robinson, A. L.: A two-dimensional
641 volatility basis set: 1. organic-aerosol mixing thermodynamics, Atmos. Chem. Phys., 11,
642 3303-3318, 2011.

643 Donahue, N. M., Henry, K. M., Mentel, T. F., Kiendler-Scharr, A., Spindler, C., Bohn, B.,
644 Brauers, T., Dorn, H. P., Fuchs, H., Tillmann, R., Wahner, A., Saathoff, H., Naumann, K.-H.,
645 Möhler, O., Leisner, T., Müller, L., Reinnig, M.-C., Hoffmann, T., Salo, K., Hallquist, M.,
646 Frosch, M., Bilde, M., Tritscher, T., Barmet, P., Praplan, A. P., DeCarlo, P. F., Dommen, J.,
647 Prévôt, A. S. H., and Baltensperger, U.: Aging of biogenic secondary organic aerosol via
648 gas-phase OH radical reactions, Proc Natl Acad Sci USA, 109, 13503-13508, 2012.

649 Ehn, M., Kleist, E., Junninen, H., Petaja, T., Lonn, G., Schobesberger, S., Dal Maso, M.,
650 Trimborn, A., Kulmala, M., Worsnop, D. R., Wahner, A., Wildt, J., and Mentel, T. F.: Gas
651 phase formation of extremely oxidized pinene reaction products in chamber and
652 ambient air, Atmos. Chem. Phys., 12, 5113-5127, 2012.

653 Ehn, M., Thornton, J. A., Kleist, E., Sipila, M., Junninen, H., Pullinen, I., Springer, M.,
654 Rubach, F., Tillmann, R., Lee, B., Lopez-Hilfiker, F., Andres, S., Acir, I.-H., Rissanen, M.,
655 Jokinen, T., Schobesberger, S., Kangasluoma, J., Kontkanen, J., Nieminen, T., Kurten, T.,
656 Nielsen, L. B., Jorgensen, S., Kjaergaard, H. G., Canagaratna, M., Dal Maso, M., Berndt, T.,
657 Petaja, T., Wahner, A., Kerminen, V.-M., Kulmala, M., Worsnop, D. R., Wildt, J., and Mentel,
658 T. F.: A large source of low-volatility secondary organic aerosol, Nature, 506, 476, 2014.

659 Ervens, B., and Volkamer, R.: Glyoxal processing by aerosol multiphase chemistry:
660 towards a kinetic modeling framework of secondary organic aerosol formation in
661 aqueous particles, Atmos. Chem. Phys., 10, 8219-8244, 2010.

662 Ervens, B., Turpin, B. J., and Weber, R. J.: Secondary organic aerosol formation in cloud
663 droplets and aqueous particles (aqSOA): a review of laboratory, field and model studies,
664 Atmos. Chem. Phys., 11, 11069-11102, 2011.

665 Goldstein, A. H., and Galbally, I. E.: Known and unexplored organic constituents in the
666 earth's atmosphere, Environ. Sci. Technol., 41, 1514-1521, 2007.

667 Hallquist, M., Wenger, J. C., Baltensperger, U., Rudich, Y., Simpson, D., Claeys, M.,
668 Dommen, J., Donahue, N. M., George, C., Goldstein, A. H., Hamilton, J. F., Herrmann, H.,
669 Hoffmann, T., Iinuma, Y., Jang, M., Jenkin, M. E., Jimenez, J. L., Kiendler-Scharr, A.,
670 Maenhaut, W., McFiggans, G., Mentel, T. F., Monod, A., Prevot, A. S. H., Seinfeld, J. H.,
671 Surratt, J. D., Szmigielski, R., and Wildt, J.: The formation, properties and impact of
672 secondary organic aerosol: current and emerging issues, Atmos. Chem. Phys., 9, 5155-
673 5235, 2009.

674 Hosny, N. A., Fitzgerald, C., Tong, C., Kalberer, M., Kuimova, M. K., and Pope, F. D.:
675 Fluorescent lifetime imaging of atmospheric aerosols: a direct probe of aerosol viscosity,
676 Faraday Discuss., 165, 343-356, 2013.

677 Iinuma, Y., Boge, O., Gnauk, T., and Herrmann, H.: Aerosol-chamber study of the alpha-
678 pinene/O_3 reaction: influence of particle acidity on aerosol yields and products, Atmos.
679 Environ., 38, 761-773, 2004.

680 Iinuma, Y., Muller, C., Berndt, T., Boge, O., Claeys, M., and Herrmann, H.: Evidence for the
681 existence of organosulfates from beta-pinene ozonolysis in ambient secondary organic
682 aerosol, Environ. Sci. Technol., 41, 6678-6683, 2007.

683 Jang, M. S., Czoschke, N. M., Lee, S., and Kamens, R. M.: Heterogeneous atmospheric
684 aerosol production by acid-catalyzed particle-phase reactions, Science, 298, 814-817,
685 2002.

686 Jaoui, M., Corse, E., Kleindienst, T. E., Offenberg, J. H., Lewandowski, M., and Edney, E. O.:
687 Analysis of secondary organic aerosol compounds from the photooxidation of d-
688 limonene in the presence of NOx and their detection in ambient PM2.5, Environ. Sci.
689 Technol., 40, 3819-3828, 2006.

690 Jimenez, J. L., Canagaratna, M. R., Donahue, N. M., Prevot, A. S. H., Zhang, Q., Kroll, J. H.,
691 DeCarlo, P. F., Allan, J. D., Coe, H., Ng, N. L., Aiken, A. C., Docherty, K. S., Ulbrich, I. M.,

692 Grieshop, A. P., Robinson, A. L., Duplissy, J., Smith, J. D., Wilson, K. R., Lanz, V. A., Hueglin,
693 C., Sun, Y. L., Tian, J., Laaksonen, A., Raatikainen, T., Rautiainen, J., Vaattovaara, P., Ehn,
694 M., Kulmala, M., Tomlinson, J. M., Collins, D. R., Cubison, M. J., Dunlea, E. J., Huffman, J. A.,
695 Onasch, T. B., Alfarra, M. R., Williams, P. I., Bower, K., Kondo, Y., Schneider, J., Drewnick,
696 F., Borrmann, S., Weimer, S., Demerjian, K., Salcedo, D., Cottrell, L., Griffin, R., Takami, A.,
697 Miyoshi, T., Hatakeyama, S., Shimono, A., Sun, J. Y., Zhang, Y. M., Dzepina, K., Kimmel, J. R.,
698 Sueper, D., Jayne, J. T., Herndon, S. C., Trimborn, A. M., Williams, L. R., Wood, E. C.,
699 Middlebrook, A. M., Kolb, C. E., Baltensperger, U., and Worsnop, D. R.: Evolution of
700 organic aerosols in the atmosphere, Science, 326, 1525-1529, 2009.

701 Kahnt, A., Iinuma, Y., Blockhuys, F., Mutzel, A., Vermeylen, R., Kleindienst, T. E., Jaoui, M.,
702 Offenberg, J. H., Lewandowski, M., Böge, O., Herrmann, H., Maenhaut, W., and Claeys, M.:
703 2-Hydroxyterpenylic acid: An oxygenated marker compound for α-pinene secondary
704 organic aerosol in ambient fine aerosol, Environ. Sci. Technol., 48, 4901-4908, 2014.

705 Kalberer, M., Sax, M., and Samburova, V.: Molecular size evolution of oligomers in
706 organic aerosols collected in urban atmospheres and generated in a smog chamber,
707 Environ. Sci. Technol., 40, 5917-5922, 2006.

708 Kampf, C. J., Waxman, E. M., Slowik, J. G., Dommen, J., Pfaffenberger, L., Praplan, A. P.,
709 Prevot, A. S. H., Baltensperger, U., Hoffmann, T., and Volkamer, R.: Effective Henry's Law
710 Partitioning and the Salting Constant of Glyoxal in Aerosols Containing Sulfate, Environ.
711 Sci. Technol., 47, 4236-4244, 2013.

712 Kolb, C. E., Cox, R. A., Abbatt, J. P. D., Ammann, M., Davis, E. J., Donaldson, D. J., Garrett, B.
713 C., George, C., Griffiths, P. T., Hanson, D. R., Kulmala, M., McFiggans, G., Pöschl, U.,
714 Riipinen, I., Rossi, M. J., Rudich, Y., Wagner, P. E., Winkler, P. M., Worsnop, D. R., and O'
715 Dowd, C. D.: An overview of current issues in the uptake of atmospheric trace gases by
716 aerosols and clouds, Atmos. Chem. Phys., 10, 10561-10605, 2010.

717 Koop, T., Bookhold, J., Shiraiwa, M., and Pöschl, U.: Glass transition and phase state of
718 organic compounds: dependency on molecular properties and implications for
719 secondary organic aerosols in the atmosphere, Phys. Chem. Chem. Phys., 13, 19238-
720 19255, 2011.

721 Kristensen, K., Cui, T., Zhang, H., Gold, A., Glasius, M., and Surratt, J. D.: Dimer esters in α-
722 pinene secondary organic aerosol: effect of hydroxyl radical, ozone, relative humidity
723 and aerosol acidity, Atmos. Chem. Phys., 14, 4201-4218, 2014.

724 Kroll, J. H., and Seinfeld, J. H.: Chemistry of secondary organic aerosol: Formation and
725 evolution of low-volatility organics in the atmosphere, Atmos. Environ., 42, 3593-3624,
726 2008.

727 Kundu, S., Fisseha, R., Putman, A. L., Rahn, T. A., and Mazzoleni, L. R.: High molecular
728 weight SOA formation during limonene ozonolysis: insights from ultrahigh-resolution
729 FT-ICR mass spectrometry characterization, Atmos. Chem. Phys., 12, 5523-5536, 2012.

730 Kuwata, M., and Martin, S. T.: Phase of atmospheric secondary organic material affects
731 its reactivity, Proc Natl Acad Sci USA, 109, 17354-17359, 2012.

732 Laskin, A., Laskin, J., and Nizkorodov, S. A.: Mass spectrometric approaches for chemical
733 characterisation of atmospheric aerosols: critical review of the most recent advances,
734 Environ. Chem., 9, 163-189, 2012a.

735 Laskin, J., Eckert, P. A., Roach, P. J., Heath, B. S., Nizkorodov, S. A., and Laskin, A.: Chemical
736 Analysis of Complex Organic Mixtures Using Reactive Nanospray Desorption
737 Electrospray Ionization Mass Spectrometry, Anal. Chem., 84, 7179-7187, 2012b.

738 Liggio, J., Li, S. M., and McLaren, R.: Heterogeneous reactions of glyoxal on particulate
739 matter: Identification of acetals and sulfate esters, Environ. Sci. Technol., 39, 1532-1541,
740 2005.

741 Lim, Y. B., Tan, Y., Perri, M. J., Seitzinger, S. P., and Turpin, B. J.: Aqueous chemistry and its
742 role in secondary organic aerosol (SOA) formation, Atmos. Chem. Phys., 10, 10521-
743 10539, 2010.

744 Lin, Y.-H., Zhang, Z., Docherty, K. S., Zhang, H., Budisulistiorini, S. H., Rubitschun, C. L.,
745 Shaw, S. L., Knipping, E. M., Edgerton, E. S., Kleindienst, T. E., Gold, A., and Surratt, J. D.:
746 Isoprene Epoxydiols as Precursors to Secondary Organic Aerosol Formation: Acid-
747 Catalyzed Reactive Uptake Studies with Authentic Compounds, Environ. Sci. Technol.,
748 46, 250-258, 2012.

749 Lin, Y.-H., Zhang, H., Pye, H. O. T., Zhang, Z., Marth, W. J., Park, S., Arashiro, M., Cui, T.,
750 Budisulistiorini, S. H., Sexton, K. G., Vizuete, W., Xie, Y., Luecken, D. J., Piletic, I. R., Edney,
751 E. O., Bartolotti, L. J., Gold, A., and Surratt, J. D.: Epoxide as a precursor to secondary
752 organic aerosol formation from isoprene photooxidation in the presence of nitrogen
753 oxides, Proc Natl Acad Sci USA, 110, 6718-6723, 2013.

754 Loza, C. L., Craven, J. S., Yee, L. D., Coggon, M. M., Schwantes, R. H., Shiraiwa, M., Zhang, X.,
755 Schilling, K. A., Ng, N. L., Canagaratna, M. R., Ziemann, P. J., Flagan, R. C., and Seinfeld, J. H.:
756 Secondary organic aerosol yields of 12-carbon alkanes, Atmos. Chem. Phys., 14, 1423-
757 1439, 2014.

758 McNeill, V. F., Woo, J. L., Kim, D. D., Schwier, A. N., Wannell, N. J., Sumner, A. J., and
759 Barakat, J. M.: Aqueous-phase secondary organic aerosol and organosulfate formation in
760 atmospheric aerosols: A modeling study, Environ. Sci. Technol., 46, 8075-8081, 2012.

761 Nguyen, T. B., Laskin, J., Laskin, A., and Nizkorodov, S. A.: Nitrogen-Containing Organic
762 Compounds and Oligomers in Secondary Organic Aerosol Formed by Photooxidation of
763 Isoprene, Environ. Sci. Technol., 45, 6908-6918, 2011.

764 Nguyen, T. B., Nizkorodov, S. A., Laskin, A., and Laskin, J.: An approach toward
765 quantification of organic compounds in complex environmental samples using high-
766 resolution electrospray ionization mass spectrometry, Analytical Methods, 5, 72-80,
767 2013.

768 Offenberg, J. H., Lewandowski, M., Edney, E. O., Kleindienst, T. E., and Jaoui, M.: Influence
769 of Aerosol Acidity on the Formation of Secondary Organic Aerosol from Biogenic
770 Precursor Hydrocarbons, Environ. Sci. Technol., 43, 7742-7747, 2009.

771 Pankow, J. F.: An absorption-model of the gas aerosol partitioning involved in the
772 formation of secondary organic aerosol, Atmos. Environ., 28, 189-193, 1994.

773 Perraud, V., Bruns, E. A., Ezell, M. J., Johnson, S. N., Yu, Y., Alexander, M. L., Zelenyuk, A.,
774 Imre, D., Chang, W. L., Dabdub, D., Pankow, J. F., and Finlayson-Pitts, B. J.:
775 Nonequilibrium atmospheric secondary organic aerosol formation and growth, Proc
776 Natl Acad Sci USA, 109, 2836-2841, 2012.

Pfrang, C., Shiraiwa, M., and Pöschl, U.: Chemical ageing and transformation of diffusivity in semi-solid multi-component organic aerosol particles, Atmos. Chem. Phys., 11, 7343-7354, 2011.

Pierce, J. R., Riipinen, I., Kulmala, M., Ehn, M., Petäjä, T., Junninen, H., Worsnop, D. R., and Donahue, N. M.: Quantification of the volatility of secondary organic compounds in ultrafine particles during nucleation events, Atmos. Chem. Phys., 11, 9019-9036, 2011.

Pöschl, U., Rudich, Y., and Ammann, M.: Kinetic model framework for aerosol and cloud surface chemistry and gas-particle interactions - Part 1: General equations, parameters, and terminology, Atmos. Chem. Phys., 7, 5989-6023, 2007.

Presto, A. A., Hartz, K. E. H., and Donahue, N. M.: Secondary organic aerosol production from terpene ozonolysis. 2. Effect of NOx concentration, Environ. Sci. Technol., 39, 7046-7054, 2005.

Renbaum-Wolff, L., Grayson, J. W., Bateman, A. P., Kuwata, K., Sellier, M., Murray, B. J., Schilling, J. E., Martin, S. T., and Bertram, A. K.: Viscosity of α-pinene secondary organic material and implications for particle growth and reactivity, Proc Natl Acad Sci USA, 110, 8014-8019, 2013.

Riipinen, I., Pierce, J. R., Yli-Juuti, T., Nieminen, T., Hakkinen, S., Ehn, M., Junninen, H., Lehtipalo, K., Petaja, T., Slowik, J., Chang, R., Shantz, N. C., Abbatt, J., Leaitch, W. R., Kerminen, V. M., Worsnop, D. R., Pandis, S. N., Donahue, N. M., and Kulmala, M.: Organic condensation: a vital link connecting aerosol formation to cloud condensation nuclei (CCN) concentrations, Atmos. Chem. Phys., 11, 3865-3878, 2011.

Sareen, N., Schwier, A. N., Shapiro, E. L., Mitroo, D., and McNeill, V. F.: Secondary organic material formed by methylglyoxal in aqueous aerosol mimics, Atmos. Chem. Phys., 10, 997-1016, 2010.

Schilling-Fahnestock, K. A., Yee, L. D., Loza, C. L., Coggon, M. M., Schwantes, R., Zhang, X., Dalleska, N. F., and Seinfeld, J. H.: Secondary Organic Aerosol Composition from C12 Alkanes, J. Phys. Chem. A, 2014.

Schobesberger, S., Junninen, H., Bianchi, F., Lonn, G., Ehn, M., Lehtipalo, K., Dommen, J., Ehrhart, S., Ortega, I. K., Franchin, A., Nieminen, T., Riccobono, F., Hutterli, M., Duplissy, J., Almeida, J., Amorim, A., Breitenlechner, M., Downard, A. J., Dunne, E. M., Flagan, R. C., Kajos, M., Keskinen, H., Kirkby, J., Kupc, A., Kuerten, A., Kurten, T., Laaksonen, A., Mathot, S., Onnela, A., Praplan, A. P., Rondo, L., Santos, F. D., Schallhart, S., Schnitzhofer, R., Sipila, M., Tome, A., Tsagkogeorgas, G., Vehkamaki, H., Wimmer, D., Baltensperger, U., Carslaw, K. S., Curtius, J., Hansel, A., Petaja, T., Kulmala, M., Donahue, N. M., and Worsnop, D. R.: Molecular understanding of atmospheric particle formation from sulfuric acid and large oxidized organic molecules, Proc Natl Acad Sci USA, 110, 17223-17228, 2013.

Shiraiwa, M., Ammann, M., Koop, T., and Pöschl, U.: Gas uptake and chemical aging of semisolid organic aerosol particles, Proc Natl Acad Sci USA, 108, 11003-11008, 2011.

Shiraiwa, M., Pfrang, C., Koop, T., and Pöschl, U.: Kinetic multi-layer model of gas-particle interactions in aerosols and clouds (KM-GAP): linking condensation, evaporation and chemical reactions of organics, oxidants and water, Atmos. Chem. Phys., 12, 2777-2794, 2012.

819 Shiraiwa, M., and Seinfeld, J. H.: Equilibration timescale of atmospheric secondary
820 organic aerosol partitioning, Geophys. Res. Lett., 39, L24801, 2012.

821 Shiraiwa, M., Yee, L. D., Schilling, K. A., Loza, C. L., Craven, J. S., Zuend, A., Ziemann, P. J.,
822 and Seinfeld, J. H.: Size distribution dynamics reveal particle-phase chemistry in organic
823 aerosol formation, Proc Natl Acad Sci USA, 110, 11746-11750, 2013a.

824 Shiraiwa, M., Zuend, A., Bertram, A. K., and Seinfeld, J. H.: Gas-particle partitioning of
825 atmospheric aerosols: interplay of physical state, non-ideal mixing and morphology,
826 Phys. Chem. Chem. Phys., 15, 11441-11453, 2013b.

827 Surratt, J. D., Murphy, S. M., Kroll, J. H., Ng, N. L., Hildebrandt, L., Sorooshian, A.,
828 Szmigielski, R., Vermeylen, R., Maenhaut, W., Claeys, M., Flagan, R. C., and Seinfeld, J. H.:
829 Chemical composition of secondary organic aerosol formed from the photooxidation of
830 isoprene, J. Phys. Chem. A, 110, 9665-9690, 2006.

831 Surratt, J. D., Gomez-Gonzalez, Y., Chan, A. W. H., Vermeylen, R., Shahgholi, M.,
832 Kleindienst, T. E., Edney, E. O., Offenberg, J. H., Lewandowski, M., Jaoui, M., Maenhaut, W.,
833 Claeys, M., Flagan, R. C., and Seinfeld, J. H.: Organosulfate formation in biogenic
834 secondary organic aerosol, J. Phys. Chem. A, 112, 8345-8378, 2008.

835 Surratt, J. D., Chan, A. W. H., Eddingsaas, N. C., Chan, M. N., Loza, C. L., Kwan, A. J., Hersey,
836 S. P., Flagan, R. C., Wennberg, P. O., and Seinfeld, J. H.: Reactive intermediates revealed in
837 secondary organic aerosol formation from isoprene, Proc Natl Acad Sci USA, 107, 6640-
838 6645, 2010.

839 Trump, E. R., and Donahue, N. M.: Oligomer formation within secondary organic
840 aerosols: equilibrium and dynamic considerations, Atmos. Chem. Phys., 14, 3691-3701,
841 2014.

842 Vaden, T. D., Imre, D., Beranek, J., Shrivastava, M., and Zelenyuk, A.: Evaporation kinetics
843 and phase of laboratory and ambient secondary organic aerosol, Proc Natl Acad Sci USA,
844 108, 2190-2195, 2011.

845 Virtanen, A., Joutsensaari, J., Koop, T., Kannosto, J., YliPirilä, P., Leskinen, J., Mäkelä, J. M.,
846 Holopainen, J. K., Pöschl, U., Kulmala, M., Worsnop, D. R., and Laaksonen, A.: An
847 amorphous solid state of biogenic secondary organic aerosol particles, Nature, 467, 824-
848 827, 2010.

849 Vogel, A. L., Äijälä, M., Corrigan, A. L., Junninen, H., Ehn, M., Petäjä, T., Worsnop, D. R.,
850 Kulmala, M., Russell, L. M., Williams, J., and Hoffmann, T.: In situ submicron organic
851 aerosol characterization at a boreal forest research station during HUMPPA-COPEC
852 2010 using soft and hard ionization mass spectrometry, Atmos. Chem. Phys., 13, 10933-
853 10950, 2013.

854 Williams, B. J., Goldstein, A. H., Kreisberg, N. M., and Hering, S. V.: In situ measurements
855 of gas/particle-phase transitions for atmospheric semivolatile organic compounds, Proc
856 Natl Acad Sci USA, 107, 6676-6681, 2010.

857 Worsnop, D. R., Morris, J. W., Shi, Q., Davidovits, P., and Kolb, C. E.: A chemical kinetic
858 model for reactive transformations of aerosol particles, Geophys. Res. Lett., 29, 57, 2002.

Xu, L., Kollman, M. S., Song, C., Shilling, J. E., and Ng, N. L.: Effects of NOx on the Volatility of Secondary Organic Aerosol from Isoprene Photooxidation, Environ. Sci. Technol., 48, 2253-2262, 2014.

Yee, L. D., Craven, J. S., Loza, C. L., Schilling, K. A., Ng, N. L., Canagaratna, M. R., Ziemann, P. J., Flagan, R. C., and Seinfeld, J. H.: Secondary organic aerosol formation from low-NO_x photooxidation of dodecane: evolution of multigeneration gas-phase chemistry and aerosol composition, J. Phys. Chem. A, 116, 6211-6230, 2012.

Zaveri, R. A., Easter, R. C., Shilling, J. E., and Seinfeld, J. H.: Modeling kinetic partitioning of secondary organic aerosol and size distribution dynamics: representing effects of volatility, phase state, and particle-phase reaction, Atmos. Chem. Phys., 14, 5153-5181, 2014.

Zhang, X., Pandis, S. N., and Seinfeld, J. H.: Diffusion-limited versus quasi-equilibrium aerosol growth, Aerosol Sci. Technol., 46, 874-885, 2012.

Zhao, R., Lee, A. K. Y., and Abbatt, J. P. D.: Investigation of Aqueous-Phase Photooxidation of Glyoxal and Methylglyoxal by Aerosol Chemical Ionization Mass Spectrometry: Observation of Hydroxyhydroperoxide Formation, J. Phys. Chem. A, 116, 6253-6263, 2012.

Zhou, S., Shiraiwa, M., McWhinney, R., Pöschl, U., and Abbatt, J. P. D.: Kinetic limitations in gas-particle reactions arising from slow diffusion in secondary organic aerosol, Faraday Discuss., 165, 391-406, 2013.

Ziemann, P. J., and Atkinson, R.: Kinetics, products, and mechanisms of secondary organic aerosol formation, Chem. Soc. Rev., 41, 6582-6605, 2012.

Zuend, A., and Seinfeld, J. H.: Modeling the gas-particle partitioning of secondary organic aerosol: the importance of liquid-liquid phase separation, Atmos. Chem. Phys., 12, 3857-3882, 2012.

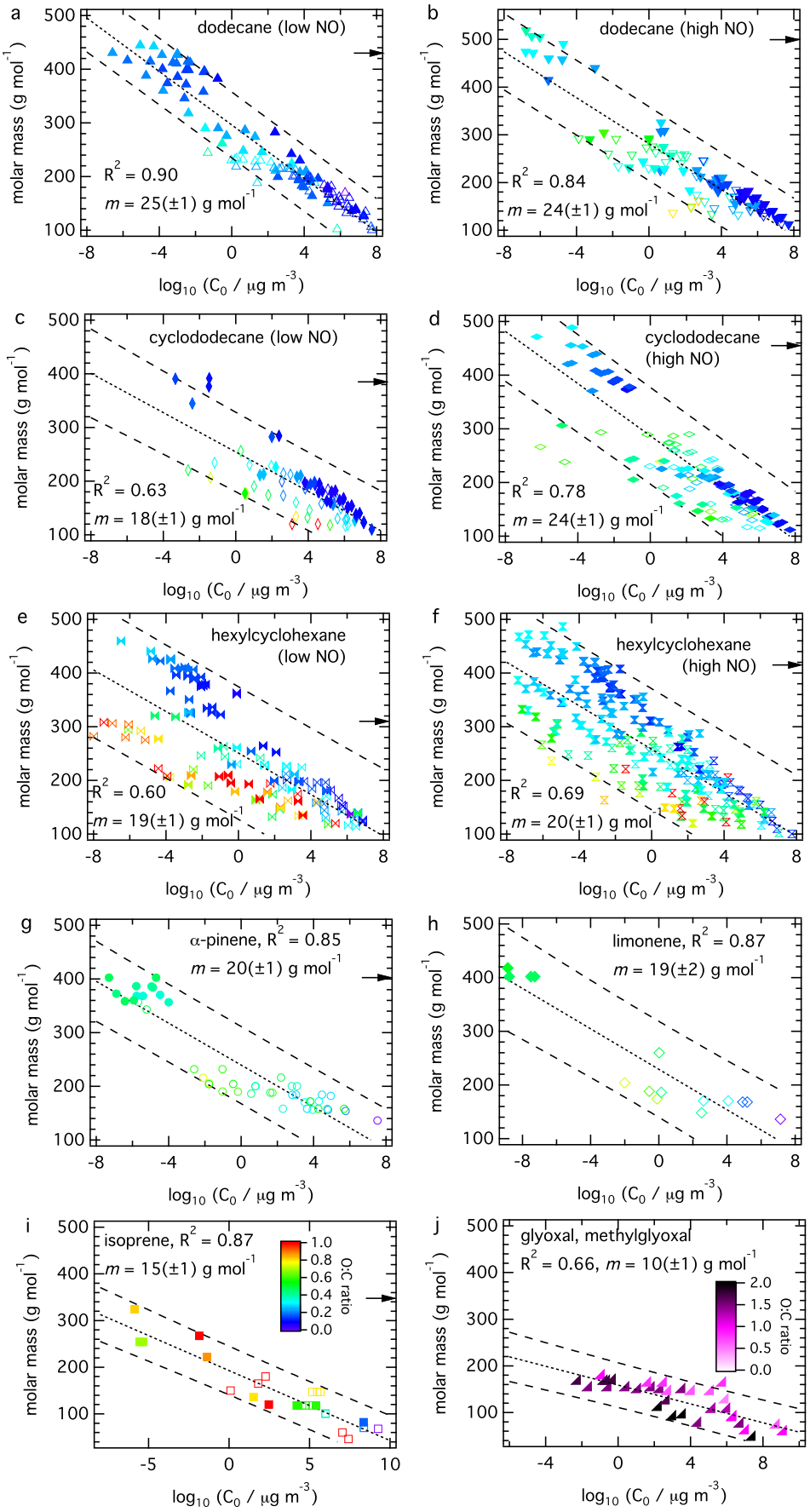
a
dodecane (low NO)
R2 = 0.90
m = 25(±1) g mol-1
b
dodecane (high NO)
R2 = 0.84
m = 24(±1) g mol-1
c
cyclododecane (low NO)
R2 = 0.63
m = 18(±1) g mol-1
d
cyclododecane (high NO)
R2 = 0.78
m = 24(±1) g mol-1
e
hexylcyclohexane (low NO)
R2 = 0.60
m = 19(±1) g mol-1
f
hexylcyclohexane (high NO)
R2 = 0.69
m = 20(±1) g mol
g
α-pinene, R2 = 0.85
m = 20(±1) g mol-1
h
limonene, R2 = 0.87
m = 19(±2) g mol-1
i
isoprene, R2 = 0.87
m = 15(±1) g mol-1
O:C ratio
j
glyoxal, methylglyoxal
R2 = 0.66, m = 10(±1) g mol-1
O:C ratio
molar mass (g mol-1)
log10 (C0 / µg m-3)

886

887 **Figure 1.** Molecular corridors of SOA evolution for different precursor compounds.
888 Molar mass vs. volatility (saturation mass concentration, C_0) at 298 K for oxidation
889 products of dodecane at low (a) and high (b) NO condition, cyclododecane at low (c)
890 and high (d) NO condition, and hexylcyclohexane at low (e) and high (f) NO
891 condition and isoprene (g), α-pinene (h), limonene (i), and glyoxal and methylglyoxal
892 (j). The open and solid markers correspond to the gas- and particle-phase products,
893 respectively, color-coded by atomic O:C ratio (note different color scale for panel j).
894 With a linear regression analysis, the coefficient of determination (R^2), fitted lines
895 (dotted lines) and their slopes (m), and prediction intervals with 95% confidence
896 (dashed lines) are shown. The arrows on the right axis indicate average molar mass
897 for isoprene and α-pinene (Kalberer et al., 2006) as well as for alkanes as measured in
898 this study.
899

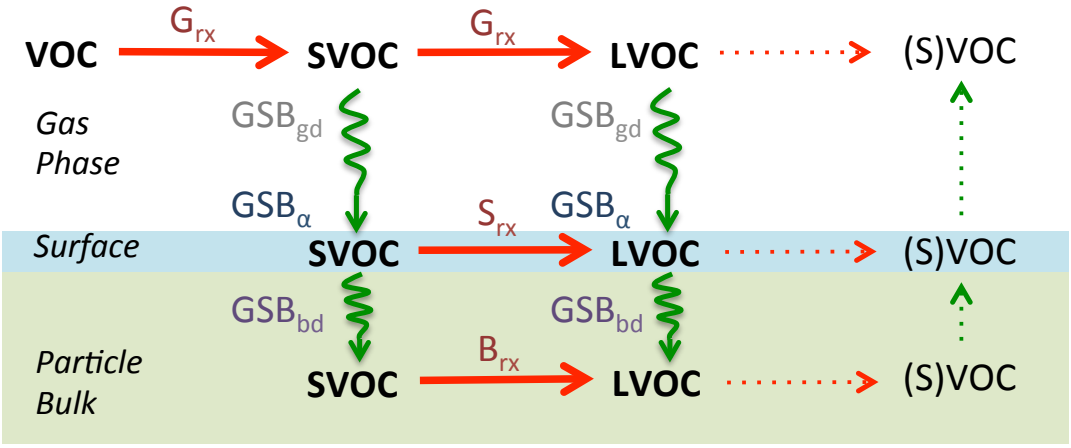

900

901 **Figure 2.** Molecular processes of SOA evolution: schematic outline of formation and
902 aging. Red and green arrows denote chemical reactions and mass transport,
903 respectively. Sequential and parallel reactions in the gas phase, at the particle surface,
904 and in the particle bulk lead to multiple generations of volatile, semi-volatile and low-
905 volatile organic compounds (VOC, SVOC, LVOC). Dotted arrows denote
906 revolatilization resulting from fragmentation reactions. Labels on arrows relate to
907 kinetic regimes outlined in subsequent figure.

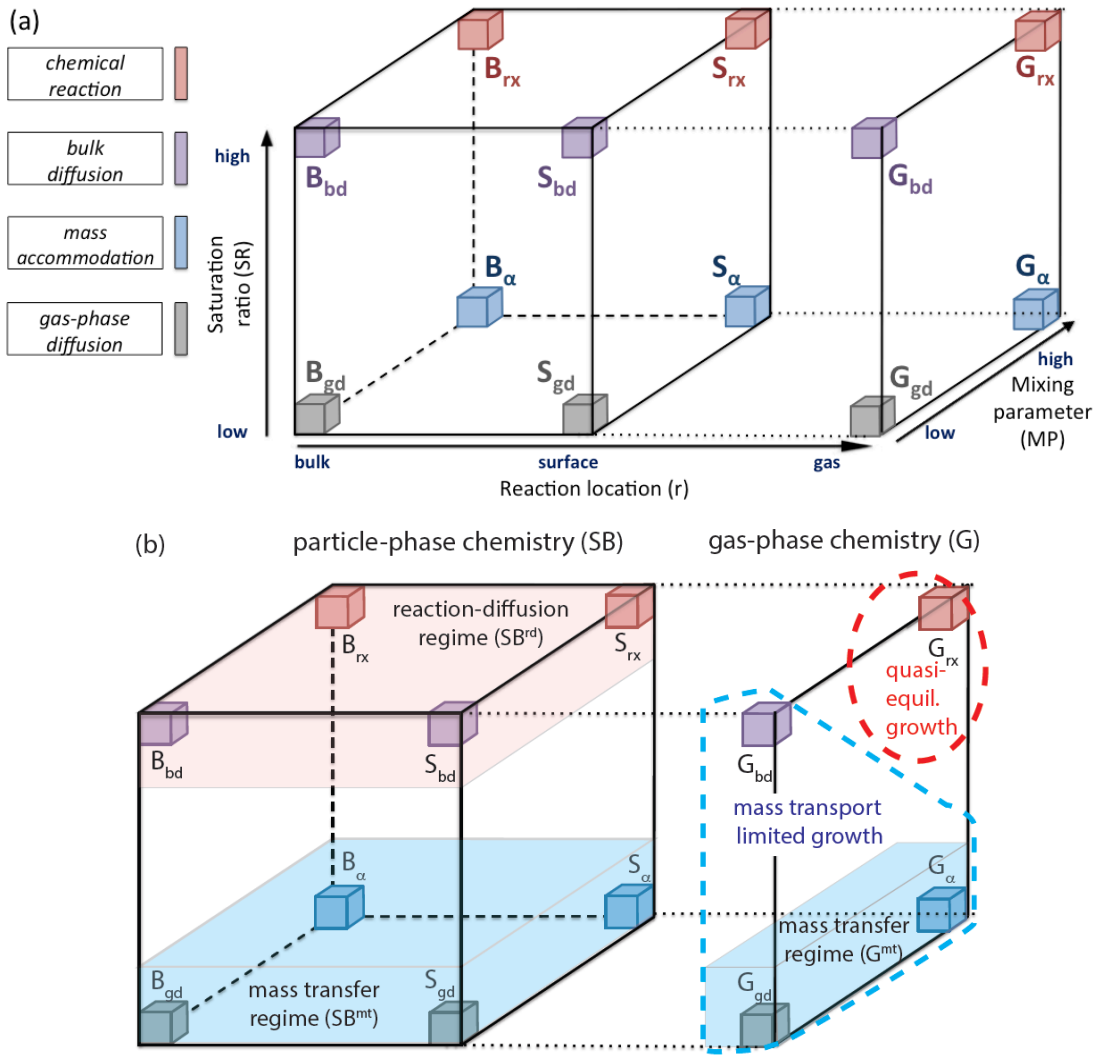

Figure 3. Kinetic regimes and limiting cases of SOA evolution mapped onto the axes of a cuboid representing reaction location, saturation ratio, and mixing parameter. (a) Horizontal edges of the cuboid (left to right) correspond to four regimes governed by chemical reaction ("rx", red), bulk diffusion ("bd", purple), mass accommodation ("α", blue), or gas-phase diffusion ("gd", grey). Each of these regimes includes three distinct limiting cases characterized by a single rate-limiting process and a dominant reaction location (particle bulk, B; surface, S; gas phase, G). (b) The left side of the cuboid can be regarded as a particle-phase chemistry regime (SB) and subdivided into a reaction-diffusion regime (SB^{rd}) and a mass transfer regime (SB^{mt}). The right side of the cuboid can be regarded as a gas-phase chemistry regime (G) and subdivided into a traditional scenario of "quasi-equilibrium growth" limited only by a gas phase reaction followed by quasi-instantaneous gas-particle partitioning (G_{rx}) and a mass-transport limited regime of "non-equilibrium growth" that may be kinetically limited by gas-to-particle mass transfer (G^{mt}) or diffusion in the particle (G_{bd}).

924

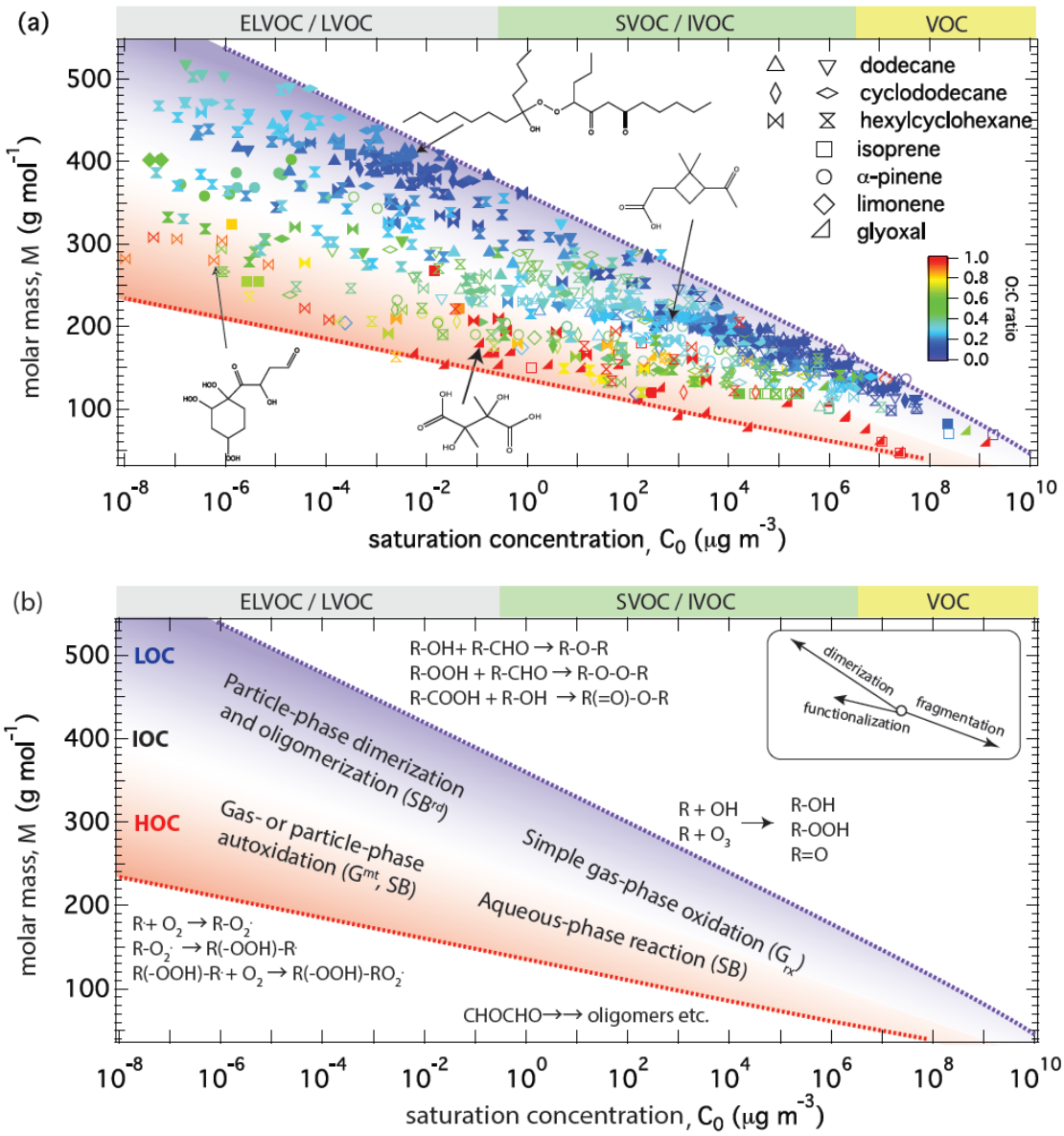

925

926 **Figure 4.** Ensemble of molecular corridors and kinetic regimes of SOA evolution. (a)
927 Molar mass vs. volatility (C_0) at 298 K for gas-phase (open) and particle-phase (solid)
928 oxidation products of anthropogenic precursors (dodecane, cyclododecane,
929 hexylcyclohexane) under low/high NO conditions, biogenic precursors (α-pinene,
930 limonene, isoprene) and aqueous-phase reaction products of glyoxal and
931 methylglyoxal. The dotted lines represent linear alkanes C_nH_{2n+2} (purple with O:C =
932 0) and sugar alcohols $C_nH_{2n+2}O_n$ (red with O:C = 1). Chemical structures of some
933 representative products are shown. (b) Characteristic reaction pathways with most
934 probable kinetic regimes. Molecular corridors consists of high, intermediate and low
935 O:C corridors (HOC, red shaded area; IOC, white area; LOC, blue shaded area). SOA
936 products evolve over the molecular corridor driven by three key reaction types of

functionalization, oligomerization and fragmentation as illustrated in the insert (note different lengths of arrows indicating different intensities of effects on volatility).

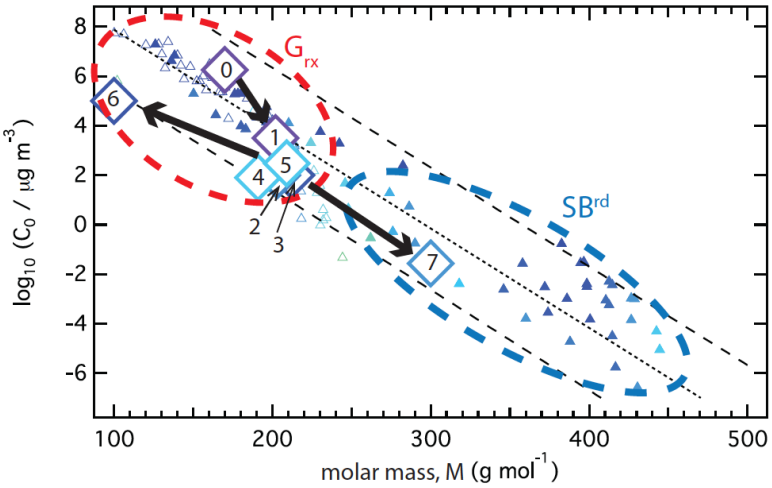

Figure 5. Evolution of reaction pathways over the molecular corridor of dodecane SOA under low NO condition. The large diamonds indicate the surrogate compounds used in the KM-GAP simulations (Appendix D; Shiraiwa et al., 2013a), including the precursor (dodecane, 0), 1st – 5th generations of surrogate products of gas-phase oxidation (1-5), gas-phase fragmentation (aldehydes, 6), and particle-phase dimerization products (7). The smaller symbols indicate identified individual products (as shown in Fig. 1a).

951 **Table 1.** Summary of analysis of identified SOA oxidation products. Number of
952 identified oxidation products N, average molar mass M_{ave}, negative slope (-
953 $dM/d\log C_0$) of fitted lines in Fig. 2 of molar mass vs. logarithm of volatility,
954 coefficients of determination R^2 as well as R^2 for O:C vs. logarithm of volatility

precursor	N	M_{ave} (g mol^{-1})	$-dM/d\log C_0$ (g mol^{-1})	R^2 (molar mass)	R^2 (O:C)
dodecane, low NO	116	429	25(±1)	0.90	0.22
dodecane, high NO	106	495	24(±1)	0.84	0.29
cyclododecane, low NO	77	384	18(±1)	0.63	0.08
cyclododecane, high NO	122	458	24(±1)	0.78	0.08
hexylcyclohexane, low NO	137	310	19(±1)	0.60	0.05
hexylcyclohexane, high NO	230	418	20(±1)	0.69	0.00
α-pinene	47	400 *	20(±1)	0.85	0.13
limonene	17	-	19(±2)	0.87	0.38
isoprene	29	350 *	15(±1)	0.87	0.09
glyoxal, methylglyoxal	35	-	10(±1)	0.66	0.16

955 * (Kalberer et al., 2006)
956

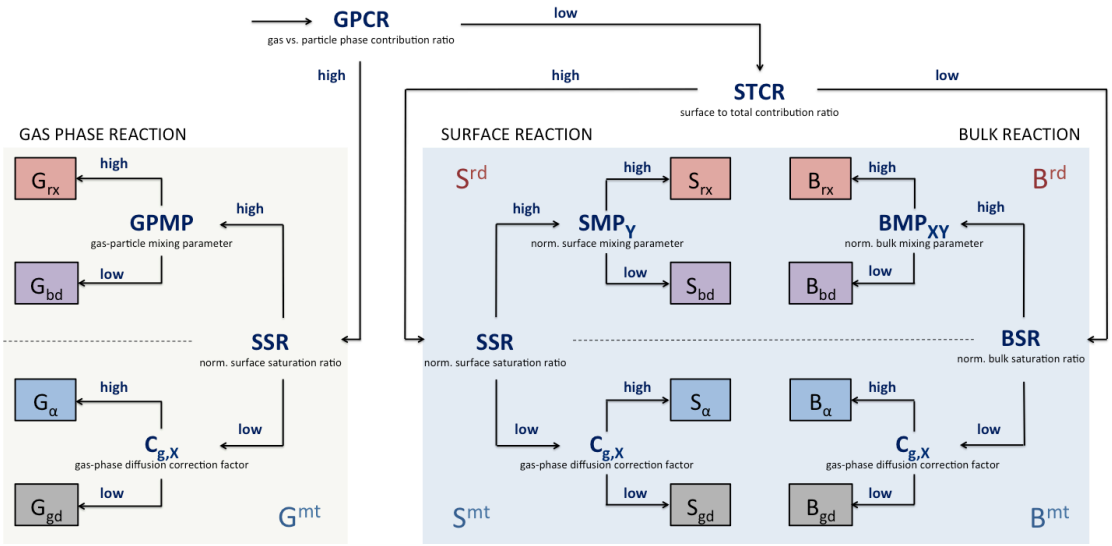

Figure A1. Decision tree for classification and distinction of limiting cases for multiphase chemical evolution of SOA. The classification is based on: 1) the location of the reaction leading to its formation, 2) its saturation ratio, and 3) its mixing parameter to assess the heterogeneity in the gas and particle phases. The resulting limiting cases are shown in the small boxes with reaction location in the gas phase (G), at the surface (S) and in the bulk (B) and limiting processes of chemical reaction (rx), bulk diffusion (bd), mass accommodation (α), and gas-phase diffusion (gd).

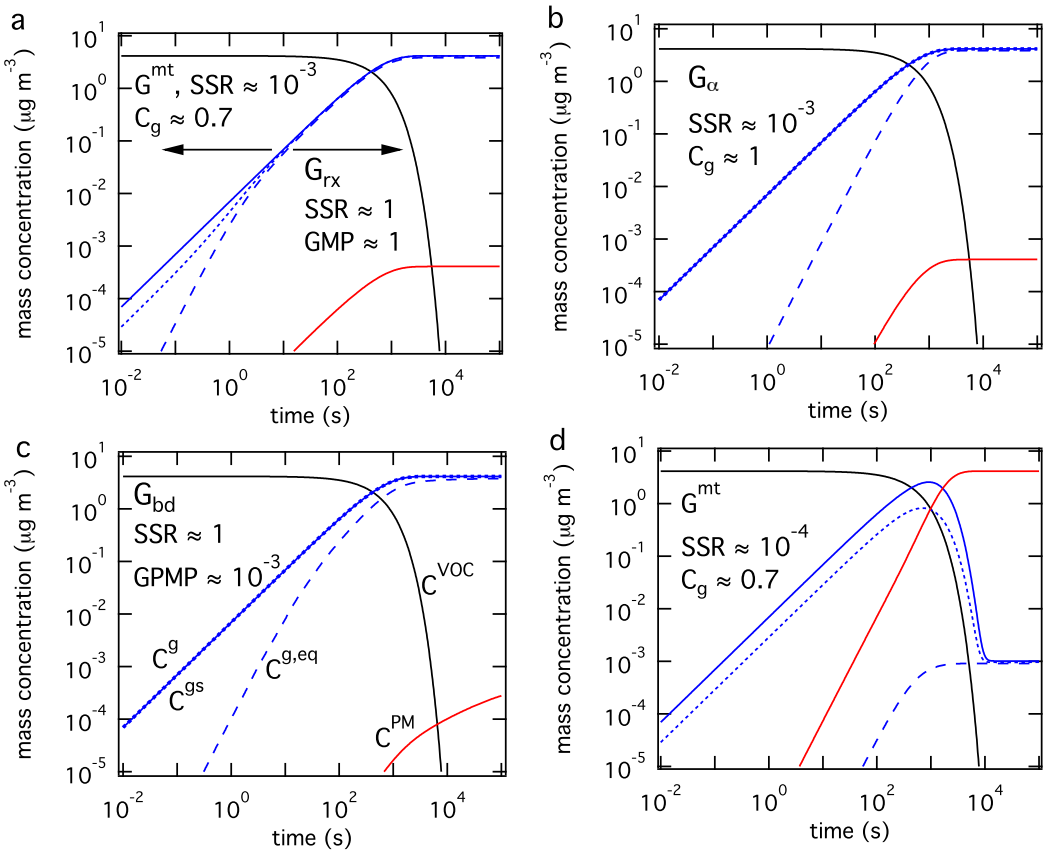

965

966 **Figure A2.** Temporal evolution of mass concentration of the hypothesized VOC
967 oxidation product in the gas phase (solid blue), in the near-surface gas phase (dotted
968 blue), in the particle phase (red), and equilibrium gas-phase concentration (dashed
969 blue). The gas-phase mass concentration of the parent VOC is shown by the black
970 line. For semi-volatile oxidation products with C^* = 10^3 μg m^{-3}, SOA growth is
971 limited by (a) gas-phase reaction (G_{rx}), (b) accommodation (G_α), and (c) bulk
972 diffusion (G_{bd}). Panel (d) shows an exemplary simulation for LVOCs with C^* = 10^{-3}
973 μg m^{-3} exhibiting kinetic limitation in the gas-particle mass transfer regime (G^{mt}).

974

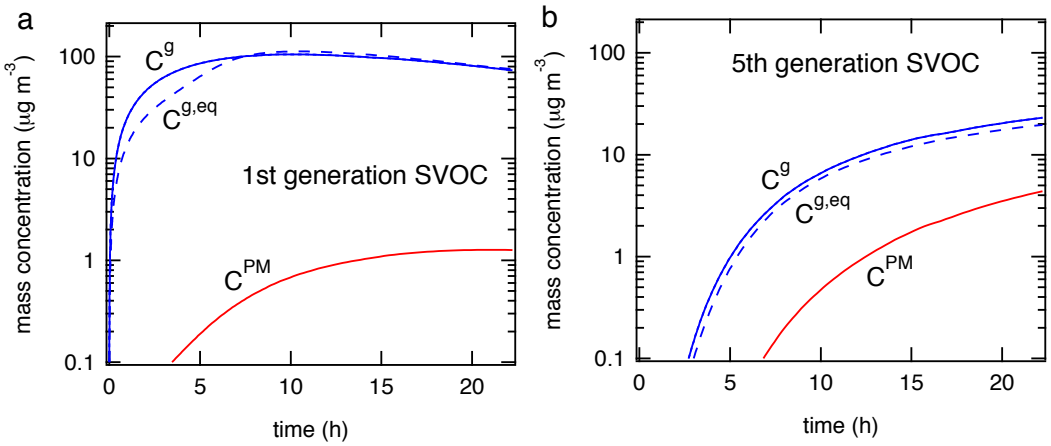

975
976 **Figure A3.** Modeling SOA formation from dodecane photooxidation. Temporal
977 evolution of mass concentration of the (a) 1st and (b) 5th generation products in the
978 gas (solid blue) and particle phases (red) and equilibrium gas-phase mass
979 concentration (dashed blue).

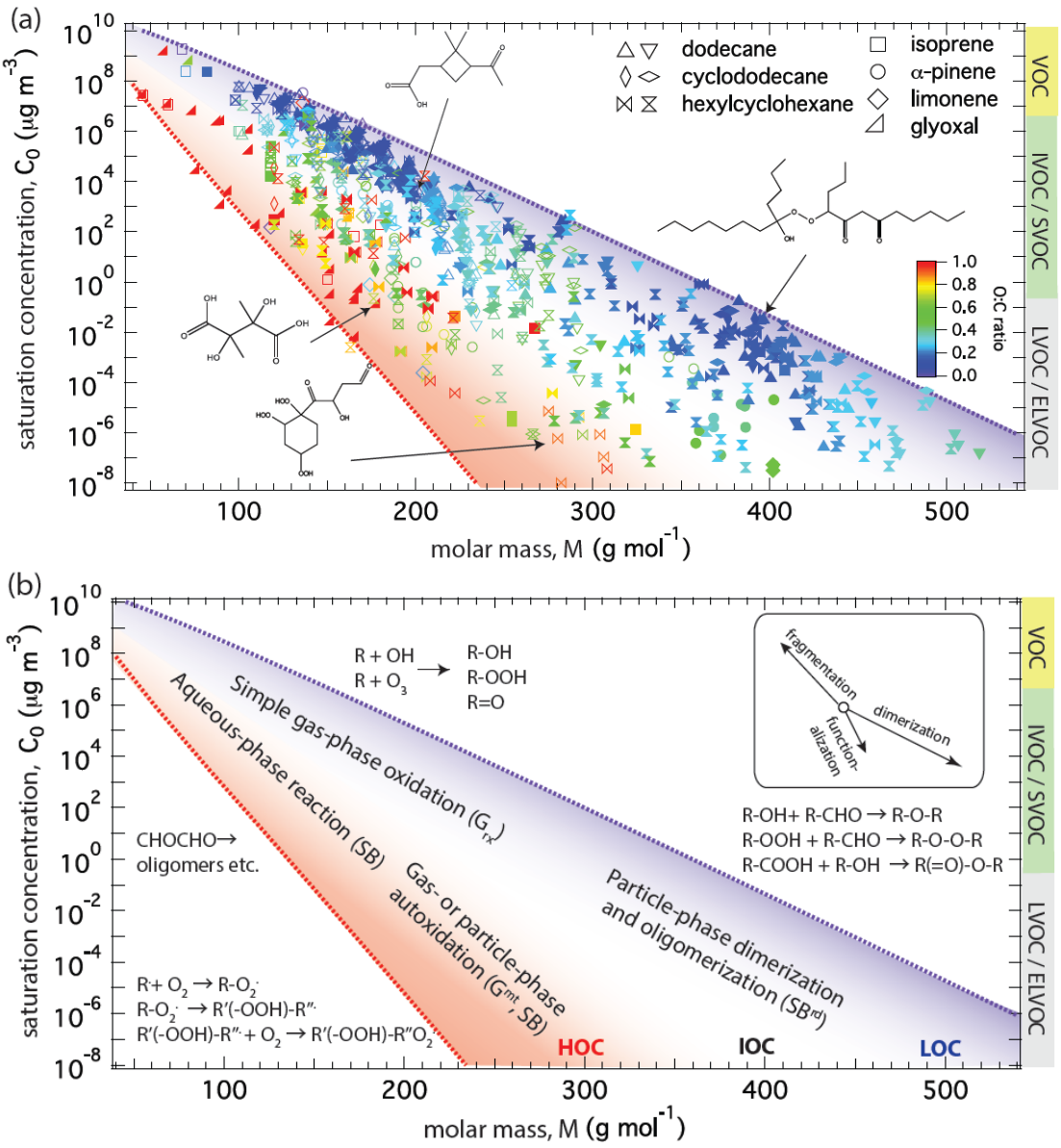

Figure A4. Alternative representation of molecular corridors (Fig. 4) displaying volatility (C_0) as a function of molar mass, which appears more straightforward to use and interpret in mechanistic studies (see Fig. 5) and for direct comparison to mass spectra. Volatility decreases as molar mass increases from left to right, and the slope $d\log C_0/dM$ is steeper for molecules with higher O:C ratio and polarity due to stronger hydrogen bonding and evaporation enthalpy.

989 **Table A1.** Experimental conditions in studies identifying oxidation products as
990 included in Figures 1 and 4.

	study	oxidants	NO	seed
dodecane	this study, Schilling-Fahnestock et al., 2014	OH	low / high	$(NH_4)_2SO_4$
cyclododecane		OH	low / high	$(NH_4)_2SO_4$
hexylcyclohexane		OH	low / high	$(NH_4)_2SO_4$
α -pinene	Docherty et al 2005	O_3	low	no seed
	Claeys et al., 2007	OH	high	no seed
	Claeys et al., 2009	OH, O_3	high / low	$(NH_4)_2SO_4$, H_2SO_4, $MgSO_4$
	Kahnt et al., 2014	O_3	high	$(NH_4)_2SO_4$, H_2SO_4
	Kristensen et al., 2014	OH, O_3	high	$(NH_4)_2SO_4$, H_2SO_4, $MgSO_4$
	Zuend & Seinfeld, 2012	O_3	low	$(NH_4)_2SO_4$
limonene	Jaoui et al., 2006	OH, O_3	high	no seed
	Kundu et al., 2012	O_3	low	no seed
isoprene	Surratt et al., 2006	OH	high / low	$(NH_4)_2SO_4$, H_2SO_4, no seed
	Surratt et al., 2010	OH	high / low	$(NH_4)_2SO_4$, H_2SO_4, no seed
	Lin et al., 2012	OH	high	no seed
	Lin et al., 2013	OH	low	$(NH_4)_2SO_4$, H_2SO_4, $MgSO_4$

991

992 **Table A2.** Properties and kinetic parameters of the VOC oxidation product used in
993 the simulations for SOA growth.

Parameter (Unit)	Description	(a)	(b)	(c)	(d)
$\alpha_{s,0}$	surface accommodation coefficient	1	10^{-3}	1	1
τ_d (s)	desorption lifetime	10^{-6}	10^{-6}	10^{-6}	10^{-6}
C_0 (μg m^{-3})	saturation mass concentration	10^3	10^3	10^3	10^{-3}
D_b (cm^2 s^{-1})	bulk diffusion coefficient	10^{-5}	10^{-5}	10^{-17}	10^{-5}
D_g (cm^2 s^{-1})	gas-phase diffusion coefficient	0.01	0.05	0.05	0.01
k_g (min^{-1})	first-order gas-phase reaction rate coefficient	0.1	0.1	0.1	0.1

994

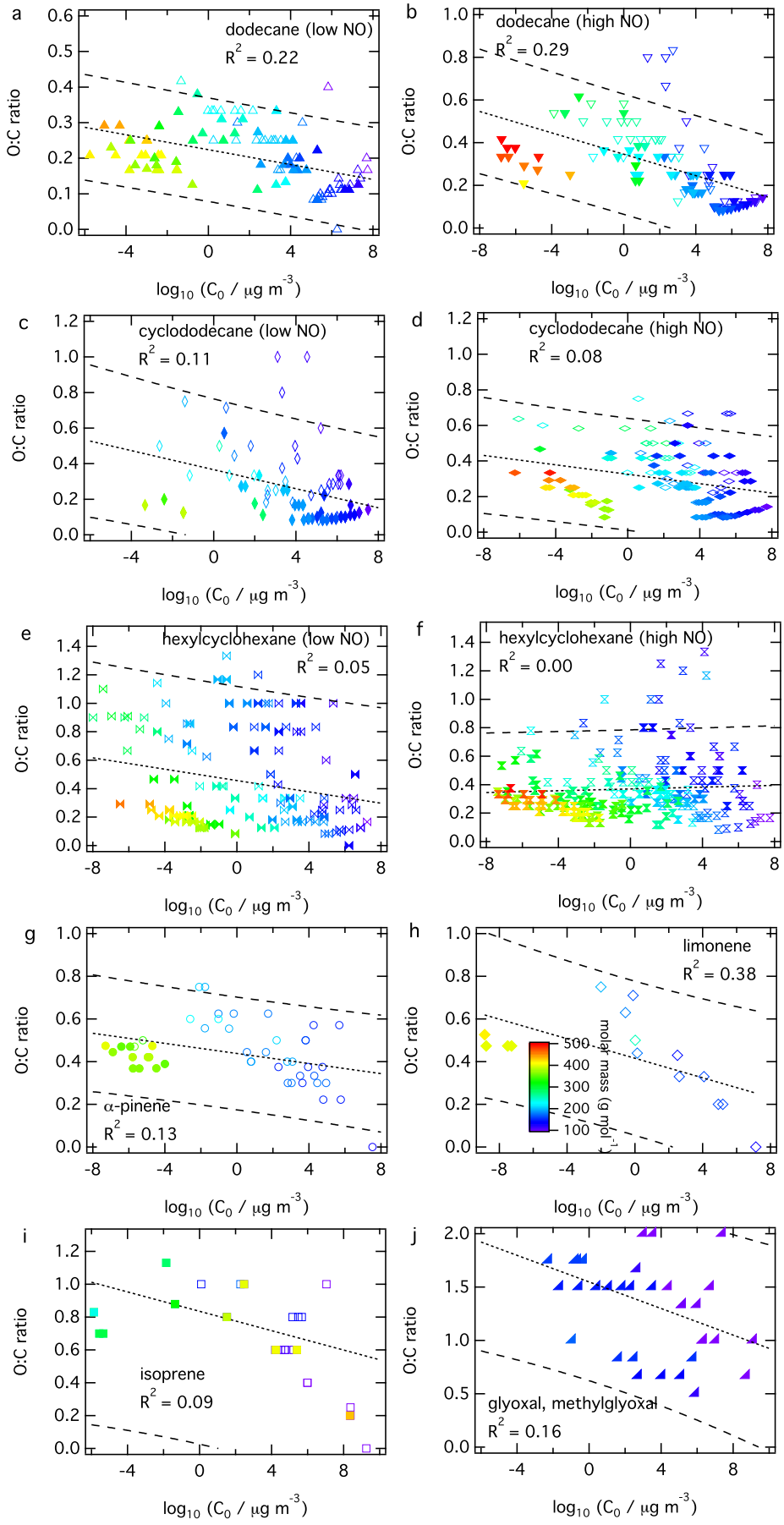
a
dodecane (low NO)
R2 = 0.22
b
dodecane (high NO)
R2 = 0.29
c
cyclododecane (low NO)
R2 = 0.11
d
cyclododecane (high NO)
R2 = 0.08
e
hexylcyclohexane (low NO)
R2 = 0.05
f
hexylcyclohexane (high NO)
R2 = 0.00
g
α-pinene
R2 = 0.13
h
limonene
R2 = 0.38
molar mass (g mol-1)
500
400
300
200
100
i
isoprene
R2 = 0.09
j
glyoxal, methylglyoxal
R2 = 0.16
O:C ratio
log10 (C0 / µg m-3)

995

Figure S1. Atomic O:C ratio vs. volatility (C_0) at 298 K for oxidation products of dodecane at low (a) and high (b) NO condition, cyclododecane at low (c) and high (d) NO condition, and hexylcyclohexane at low (e) and high (f) NO condition and isoprene (g), α-pinene (h), limonene (i), and glyoxal and methylglyoxal (j). The solid and open markers, color-coded with molar mass (g mol^{-1}), correspond to the gas- and particle-phase products, respectively. With a linear regression analysis, the correlation between both quantities has been evaluated (dotted lines) with coefficients of determination (R^2), including prediction intervals at the 95 % confidence level (dashed lines).

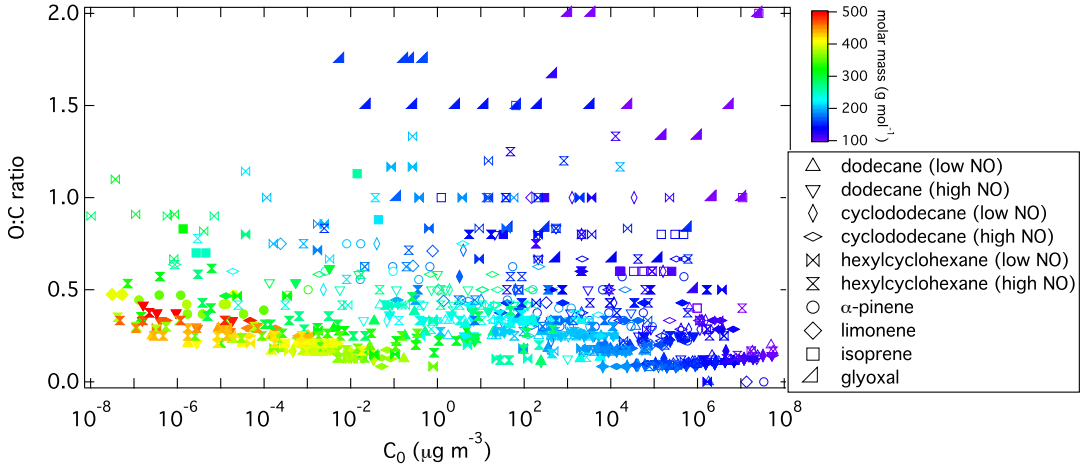

Figure S2. Summary of O:C ratio vs. C_0 for dodecane, cyclododecane, hyxylcyclohexane, α-pinene, limonene, isoprene, and glyoxal. The solid and open markers, color-coded with molar mass (g mol^{-1}), correspond to the gas- and particle-phase products, respectively.